

1 **Spring tropical cyclones modulate near-surface isotopic compositions of**
2 **atmospheric water vapour at Kathmandu, Nepal**

3 Niranjan Adhikari^{1,2}, Jing Gao^{1,3,*}, Aibin Zhao¹, Tianli Xu^{1,4} Manli Chen^{1,3},
4 Xiaowei Niu¹, Tandong Yao^{1,3}

5 ¹ *State Key Laboratory of Tibetan Plateau Earth System, Resources and Environment, Institute*
6 *of Tibetan Plateau Research, Chinese Academy of Sciences, Beijing 100101, China*

7 ² *University of Chinese Academy of Sciences, Beijing 100049, China*

8 ³ *Lanzhou University, Lanzhou 733000, China*

9 ⁴ *Kathmandu Centre for Research and Education, Chinese Academy of Sciences –Tribhuvan*
10 *University, Kirtipur 44613, Kathmandu, Nepal*

11 * Correspondence to: Jing Gao, E-mail: gaojing@itpcas.ac.cn

12
13 **Abstract**

14 While westerlies are recognized as a significant moisture transport in Nepal during the
15 pre-monsoon season, precipitation is also attributed to moisture from cyclones originating in the
16 Bay of Bengal (BoB) or the Arabian Sea (AS). Tropical cyclones exhibit negative isotopic values
17 in both precipitation and atmospheric water vapour; however, the factors influencing isotopic
18 fractionation during tropical cyclones remain poorly understood. We present the results of
19 continuous measurements of the isotopic composition of atmospheric water vapour ($\delta^{18}\text{O}_v$, δD_v ,
20 and d-excess_v) at Kathmandu from 7 May to 7 June 2021 during two pre-monsoon cyclones;
21 cyclone Tauktae formed over the Arabian Sea, and cyclone Yaas formed over the Bay of Bengal.
22 Our study reveals that tropical cyclones originating from the BoB and the AS during the pre-

23 monsoon season modulate isotopic signals of near-surface atmospheric water vapour in Nepal.
24 Comparing conditions before and after, we observed a significant depletion of $\delta^{18}\text{O}_v$ and δD_v
25 during both cyclones, attributed to changes in moisture sources (local vs. marine). Convective
26 activity plays a pivotal role in the variability of $\delta^{18}\text{O}_v$ and δD_v during both cyclones, confirmed
27 by the spatial variations of outgoing longwave radiation (OLR) and regional precipitation during
28 both cyclones. We also found a significant negative correlation between $\delta^{18}\text{O}_v/\delta\text{D}_v$ and rainfall
29 amount along the trajectories during cyclone Tauktae, probably resulting from integrated
30 upstream processes linked to the earlier Rayleigh distillation of water vapour via rainfall, rather
31 than local rainfall. The decrease in $\delta^{18}\text{O}_v/\delta\text{D}_v$ during cyclone Yaas is associated with the
32 intensified convection and moisture convergence at the measurement site, while the lower cloud
33 top temperatures (CTT) and lower cloud top pressure (CTP) during intense convection contribute
34 to higher d-excess values at the final stage of cyclone Yaas. This characteristic is missing during
35 cyclone Tauktae. Our results shed light on key processes governing the isotopic composition of
36 atmospheric water vapour at Kathmandu with implications for the monsoon moisture transport
37 and paleoclimate reconstructions of tropical cyclone activity.

38 Keywords: Cyclones; Isotopic composition of atmospheric water vapour; Convection; Moisture
39 convergence; Kathmandu

40

41

42

43 **1 Introduction**

44 Although the Indian summer monsoon accounts for more than 80 % of annual rainfall in
45 Nepal, agricultural activities also rely on precipitation in the pre-monsoon season. Pre-
46 monsoonal rainfall in Nepal is often associated with cyclonic events that provide precipitation to
47 support the timely planting of monsoonal crops. Previous studies have suggested that extreme
48 precipitation in Nepal is mostly fuelled by moisture from the Arabian Sea (AS) and the Bay of
49 Bengal (BoB) (Bohlinger et al., 2017; Boschi and Lucarini, 2019). Higher sea surface
50 temperatures and the westward movement of tropical cyclones formed over the Western Pacific
51 result in cyclones being formed over the BoB and the AS (Mohapatra et al., 2016). The number
52 of cyclones in the AS has increased recently compared to the number of cyclones in the BoB
53 (Pandya et al., 2021). According to the International Best Track Archive for Climate Stewardship
54 (IBTrACS) project (Knapp et al., 2010), in 2019 three cyclones originated in the BoB and five
55 cyclones originated in the AS, due to a rise in sea surface temperature lengthening the cyclone
56 decay period (Li and Chakraborty, 2020). Usually, the impact of cyclones formed over the AS is
57 restricted to the nearest coastal regions. However, in recent years this appears to have changed as
58 cyclones are forming back-to-back over the AS and affecting the entire Indian subcontinent
59 including surrounding regions (Li and Chakraborty, 2020). Cyclone Tauktae affected the
60 livelihoods of people both near the coast and further inland during the pre-monsoon season of
61 2021 (Pandya et al., 2021). The impacts of cyclone Yaas after cyclone Tauktae were also felt in
62 Nepal, where it triggered flooding and landslides in several parts of the country
63 (<https://floodlist.com/asia/nepal-flood-landslide-may-2021/>). As both cyclones hit in short
64 succession, this led to severe agricultural damage in several parts of India at a critical time when
65 farmers were preparing to sow their rice paddies ahead of the monsoon season

66 (<https://reliefweb.int/organization/acaps>). In Nepal, the damage due to Yaas was mostly limited
67 to the Terai regions which experienced intense and continuous rainfall
68 (<https://kathmandupost.com/>). Moisture flux associated with cyclones generally extends over a
69 large area and causes moderate to heavy precipitation along the cyclone path and on the nearest
70 land mass (Chan et al., 2022; Rajeev and Mishra, 2022). It is therefore essential to understand the
71 moisture transport processes of these extreme rainfall events on atmospheric water vapour.

72 With climate change, the amount of water vapour in the atmosphere is also expected to
73 increase, creating scientific interest in the impact of atmospheric water vapour on changing
74 moisture patterns (Hoffmann et al., 2005). The isotopic composition of atmospheric water
75 vapour ($\delta^{18}\text{O}_v$, δD_v , and $d\text{-excess}_v$) contains comprehensive information about the history of
76 moisture exchange (Noone, 2012; Payne et al., 2007; Risi et al., 2008; Worden et al., 2007).
77 Several studies have shown that the isotopic composition is an effective indicator of cyclone
78 activity (Munksgaard et al., 2015; Sun et al., 2022) including cyclone evolution and structure
79 (Lawrence et al., 2002). The atmospheric water vapour and precipitation associated with tropical
80 cyclones tend to have extremely depleted isotopic compositions compared to monsoonal rain
81 (Chen et al., 2021; Jackisch et al., 2022; Munksgaard et al., 2015; Sánchez-Murillo et al., 2019),
82 which may be due to the high condensation efficiency and substantial fractionation associated
83 with cyclones. A few studies found a systematic depletion of heavy isotopes towards the cyclone
84 eye (Lawrence et al., 2002, 1998; Lawrence and Gedzelman, 1996; Sun et al., 2022; Xu et al.,
85 2019). For example, during cyclone Shanshan, Fudeyasu (2008) observed that isotopic depletion
86 in precipitation and water vapour increased radially inward in the cyclone's outer region, likely
87 due to a rainout effect. A study conducted in north-eastern Australia during cyclone Ita in April
88 2014 underlined the role of synoptic-scale meteorological settings in determining the isotopic

89 variability of atmospheric water vapour (Munksgaard et al., 2015). In Fuzhou, China, Xu et al.,
90 (2019) reported a significant depletion in typhoon rain $\delta^{18}\text{O}$ related to the combined effect of
91 large-scale convection, high condensation efficiency, and recycling of isotopically depleted
92 vapour in the rain shield area. Sánchez-Murillo et al., (2019) highlighted the role of convective
93 and stratiform activity as well as precipitation type and amount. The impact of high stratiform
94 fractions and deep convection on isotopic depletion in precipitation during typhoon Lekima was
95 confirmed by Han et al., (2021).

96 Although several studies have examined the isotopic variation of event-based
97 precipitation in Nepal (Acharya et al., 2020; Adhikari et al., 2020; Chhetri et al., 2014), there
98 remains a knowledge gap regarding the isotopic response of atmospheric water vapour during
99 cyclone events. We present for the first time the evolution of the isotopic composition of
100 atmospheric water vapour ($\delta^{18}\text{O}_v$, δD_v , and d-excess) in Kathmandu during two pre-monsoon
101 cyclone events. Isotopic data were collected in 2021, from one week before to one week after the
102 cyclones. A substantial influence of these cyclone events on the sampling site for several days
103 was apparent in the isotopic composition of atmospheric water vapour, showcasing a marked
104 depletion in comparison to normal days. This allowed us to scrutinize fluctuations in isotopic
105 composition with a high temporal resolution and to investigate the atmospheric processes
106 associated with cyclone events that lead to significant depletion in isotopic composition at
107 diurnal scales.

108 **2 Data and methods**

109 **2.1 Site description**

110 The Kathmandu station lies on the southern slope of the Himalayas ($27^{\circ}42' \text{ N}$, $85^{\circ}20' \text{ E}$)
111 at an altitude of approximately 1400 m above sea level. Based on an 18-year-long record from

112 the Department of Hydrology and Meteorology, Government of Nepal (2001 to 2018), this
113 region has an average annual temperature of 19° C and average annual precipitation amount of
114 about 1500 mm, with ~78% of the annual rainfall occurring in the monsoon season from June to
115 September (Adhikari et al., 2020). About 16 % of annual rainfall in Kathmandu occurs in the
116 pre-monsoon season (March to May) with air temperature ranging from 13 to 28° C and an
117 average relative humidity (RH) of 67 %. Advection of the southern branch of westerlies and
118 evaporation from nearby water bodies are the main contributors to pre-monsoonal precipitation
119 (Yu et al., 2015; Chhetri et al., 2014). These arid westerlies, resulted in diminished temperature
120 and relative humidity (RH) within the region while a substantial presence of moisture was
121 observed over extensive areas encompassing the BoB, the AS, India, and surrounding regions
122 including our sampling site during our study period. Figure S1 shows the elevated specific
123 humidity levels at 850 from May 7 to June 7, 2021.

124

125 **2.2 The evolution of cyclones Tauktae and Yaas and weather conditions at** 126 **Kathmandu**

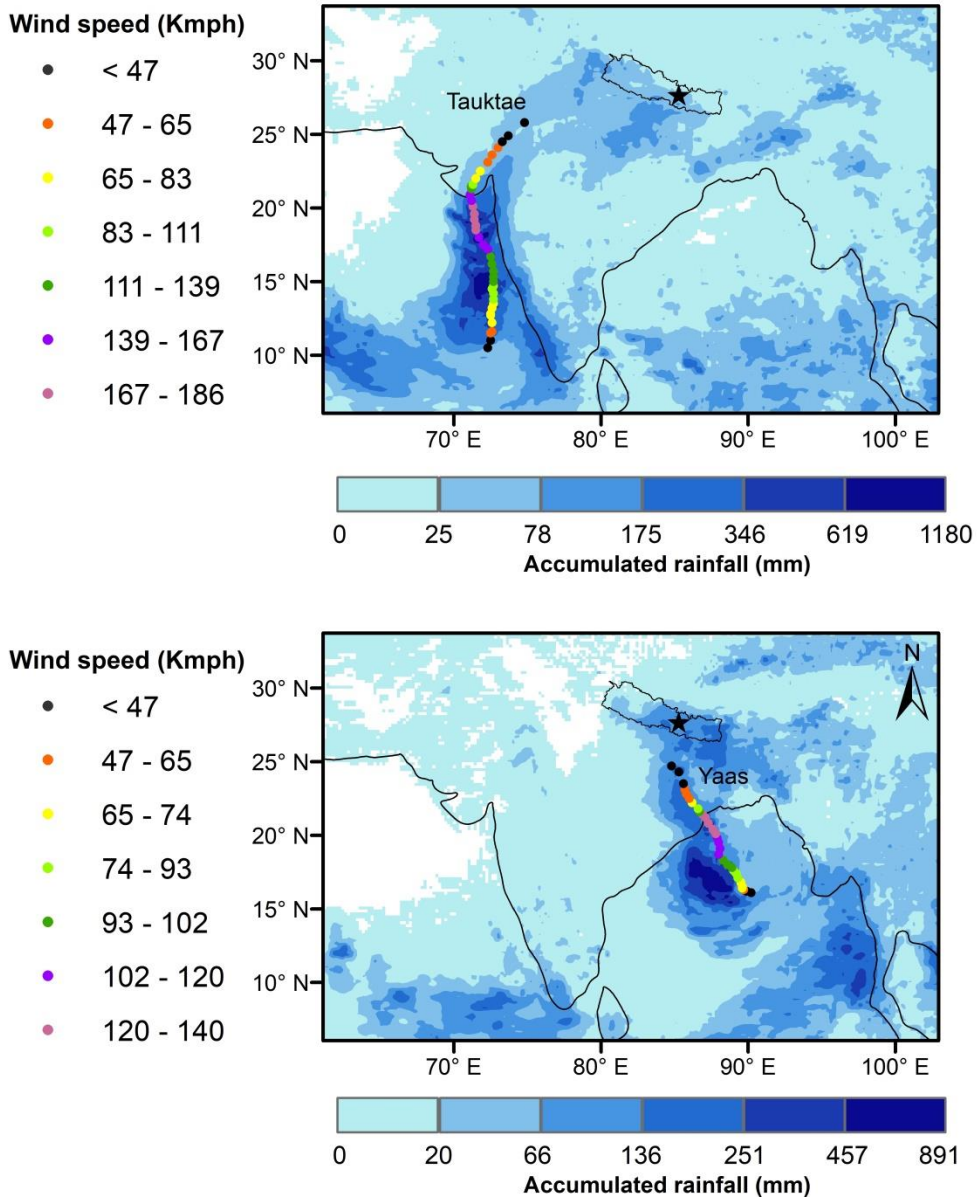
127 Cyclone Tauktae developed as a tropical disturbance on 13 May 2021 over the AS,
128 evolved into a deep depression by 14 May, moved north, and gradually intensified before turning
129 into a cyclonic storm with wind speeds reaching 75 km/h on that same day (Pandya et al., 2021).
130 After making landfall in the Gir-Somnath district of Gujarat, Tauktae continued to strengthen
131 and was classified as an extremely severe cyclonic storm on 17 May reaching maximum wind
132 speeds of 185 km/h (Verma and Gupta, 2021; Pandya et al., 2021). Tauktae weakened into a low
133 depression on 18 May 2021 at 20:30 h Indian Local Time (ILT) and finally dissipated one day
134 later. Due to its large convective area, it brought heavy rainfall to different regions of India and
135 Nepal.

136 The signal of cyclone Tauktae was first detected at the Kathmandu site on 19 May at
137 approximately 03:00 local time (LT), followed by light drizzle. The recorded air temperature was
138 about 22°C, and the relative humidity (RH) was approximately 72%. Within 16 hours, the RH
139 increased from 72% to 91%, while the temperature dropped from 22°C to around 19°C. The
140 maximum RH and minimum temperature were observed on 21 May around 04:00 h LT, reaching
141 92% and 17°C, respectively.

142 Cyclone Yaas started out as a depression over the BoB on 22 May 2021 at 08:30 h ILT
143 and gradually intensified into a deep depression before turning into a cyclonic storm on 24 May
144 at 05:30 h ILT as it moved northeast (Paul and Chowdhury, 2021). The corresponding wind
145 speed and central pressure were recorded as 65 km/h and 990 hPa, respectively. On 24 May
146 around 23:30 h ILT, it intensified into a severe cyclonic storm with wind speeds ranging from 92
147 to 111 km/h before becoming a very severe cyclonic storm on 25 May at 17:30 h ILT with wind
148 speeds from 120 km/h to 139 km/h. It made landfall north of Odisha on 26 May with maximum
149 sustained wind speeds of 130 km/h to 140 km/h and progressively weakened into a depression on
150 27 May before dissipating over northern India on 28 May.

151 The Kathmandu weather station recorded a total of 59.6 mm of precipitation during
152 cyclone Yaas. Intermittent small patches of rainfall commenced on 25 May at 11:00h LT. The
153 main cyclone event occurred from 26 May at 01:00h LT to 29 May at 01:00h LT. Throughout
154 this period, the ground-level RH fluctuated between 84% and 93%, while surface temperature
155 varied between 18°C and 22°C. Notably, all RH values exceeded 80% from 25 May around
156 22:00 h LT to 29 May at 10:00 h LT.

157 Wind speeds, pressure, and cyclone eye location information (3-hour resolution) were
158 retrieved from the best track data of tropical cyclonic disturbances over the north Indian Ocean
159 (available at <https://rsmcnewdelhi.imd.gov.in/>) monitored by India Meteorological Department
160 (IMD). The latter was used to calculate the spatial distance between the cyclone's eye and our
161 measurement location. Figure 1 illustrates the intensity and cumulative rainfall along the paths of
162 the cyclones. A characteristic of both cyclones is the occurrence of rainout along their
163 trajectories, persisting as they move inland.



164

165 **Figure 1** The intensity and track of cyclone Tauktae (Upper panel) and Yaas (Bottom
 166 panel) along with accumulated rainfall during Tauktae (from 14 to 20 May 2021) and Yaas
 167 (24 to 28 May 2021). The intensity and track of cyclones were retrieved from the best track
 168 data of tropical cyclonic disturbance over the north Indian Ocean monitored by IMD and

169 **rainfall data was retrieved from the Integrated Multi-satellite Retrievals provided by the**
170 **Global Precipitation Measurement program (GPM, IMERG dataset).**

171 **2.3 Isotope measurements**

172 Near-surface $\delta^{18}\text{O}_v$ and δD_v were measured continuously using a Picarro L2130-i
173 analyser based on wavelength-scanned cavity ring-down spectroscopy (WS-CRDS) (Brand et al.,
174 2009), located at the Kathmandu Centre for Research and Education (KCRE), Nepal. The
175 sampling inlet consisting of a heated copper tube mounted 7 m above the ground protected with a
176 plastic hood and a 10 L min^{-1} pump transported the sample from the inlet to the analyser. The
177 automated standard delivery module (SDM) was used for calibration, with each calibration made
178 using two reference standards calibrated against Vienna Standard Mean Ocean Water
179 (VSMOW), covering the isotopic ranges of ambient water vapour at Kathmandu. Each reference
180 standard was measured continuously for a total of 75 min each day at three different humidity
181 levels (25 minutes per level). The dry air passed through Drierite™ desiccant (Merck, Germany)
182 and was delivered to the Picarro analyser for standard measurements. The isotopic composition
183 of atmospheric water vapour is reported as parts per thousand (‰) relative to VSMOW using

$$184 \quad \delta^* = (R_A / R_S - 1) \times 1000 \text{ [‰]}, \quad (1)$$

185
186 where δ^* represents either δD_v or $\delta^{18}\text{O}_v$, and R_A and R_S denote the ratios of heavy to light
187 isotopes ($^{18}\text{O}/^{16}\text{O}$ or D/H) in the sample and standard, respectively (Kendall & Caldwell, 1998;
188 Yoshimura, 2015). As suggested by Dansgaard, (1964), deuterium excess ($\text{d-excess}_v = \delta\text{D}_v - 8 \times \delta^{18}\text{O}_v$)
189 is used as a tracer for moisture source conditions (Liu et al., 2008; Tian et al., 2001). The
190 detailed calibration procedures are outlined in the supplementary material, with the humidity-
191 isotopes response function presented in Figure S2 and all calibration data shown in Figure S3.

192 We examined the hourly isotopic composition of atmospheric water vapour between 7 May and
193 7 June 2021, covering the Tauktae and Yaas cyclones including one week on either side.

194 **2.4 Meteorological data**

195 An automated weather station (AWS, Davis Vantage Pro2) continuously measured air
196 temperature, relative humidity, dew point temperature, wind speed and direction, rainfall
197 amount, surface pressure, etc. at one-minute intervals from 7 May to 7 June 2021.

198 We used the Integrated Multi-satellite Retrievals provided by the Global Precipitation
199 Measurement program (GPM, IMERG dataset) with a spatial resolution of 0.1° for latitude and
200 longitude (Huffman et al., 2017) to analyse the regional rainfall intensity before, during, and
201 after the cyclone events. These high-resolution data allow for the identification of convective
202 rainfall areas and the passage of tropical cyclones (Jackisch et al., 2022). They have been used
203 previously to depict cyclone tracks and associated rainfall intensities (Gaona et al., 2018;
204 Jackisch et al., 2022; Villarini et al., 2011).

205 We further acquired data on outgoing longwave radiation (OLR), zonal and meridional
206 winds, specific humidity, vertical velocity, pressure, vertical distribution of relative humidity and
207 temperature from ERA5 datasets (Herbash et al., 2020). The data has a spatial resolution of 0.25°
208 based on longitude-latitude grids (<https://cds.climate.copernicus.eu/>). OLR data has already been
209 used as an index of tropical convection (Liebmann and Smith, 1996). Additionally, we used
210 cloud-top pressure (CTP) and cloud-top temperature (CTT) data from MERRA-2 Reanalysis
211 datasets retrieved from <https://giovanni.gsfc.nasa.gov/>, with a spatial resolution for $0.5^\circ \times 0.625^\circ$,
212 as indicators of convective intensity.

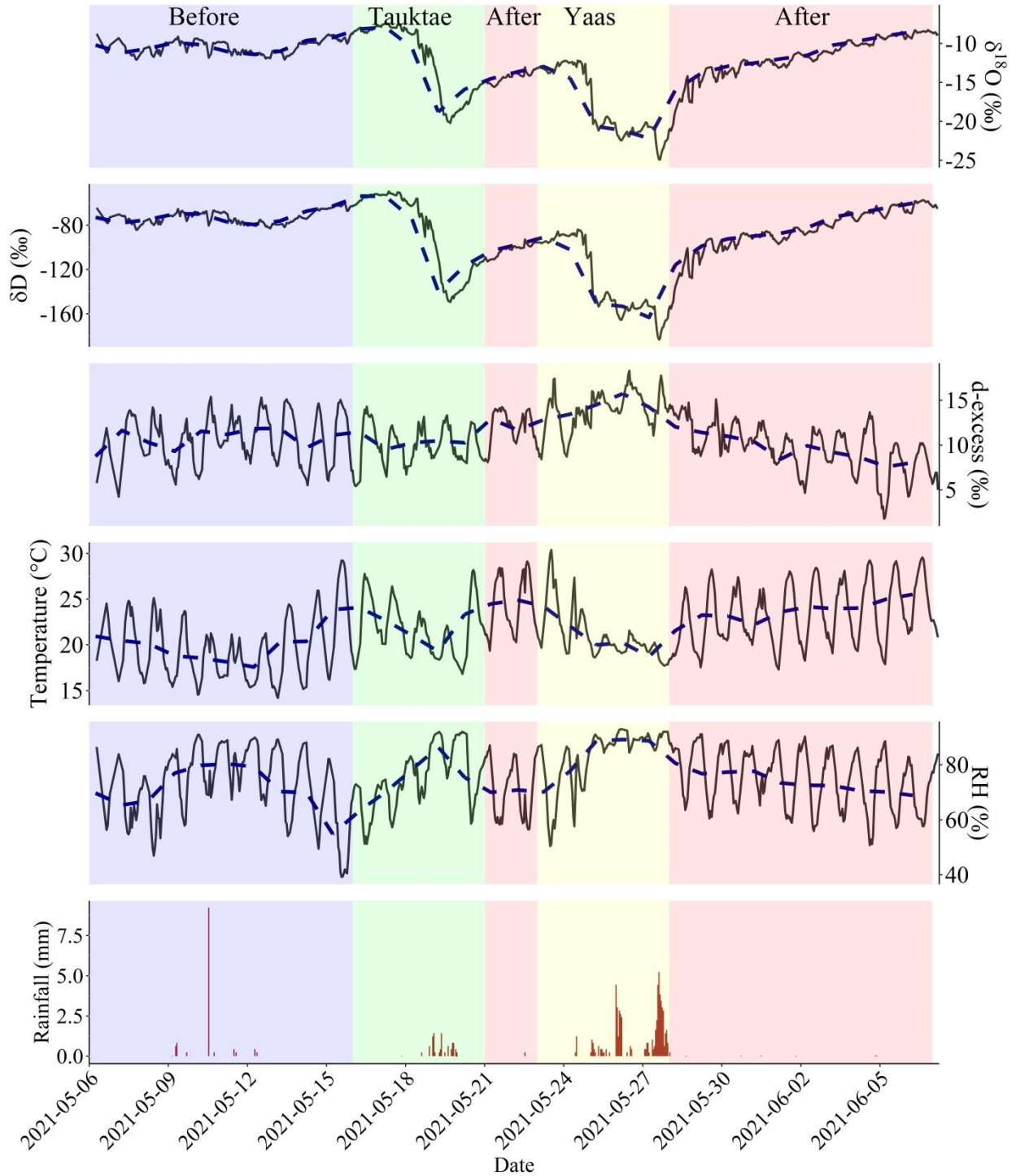
213 **2.5 Moisture backward trajectory analysis**

214 To assess the influence of moisture transport history on the isotopic composition of
215 atmospheric water vapour before, during, and after the cyclone events, we analysed five-day
216 moisture backward trajectories that terminated at the sampling site using the Hybrid Single-
217 Particle Lagrangian Integrated Trajectory (HYSPLIT) model (Draxler and Hess, 1997). The
218 Global Data Assimilation System (GDAS) with a spatial resolution of 1° (Kleist et al., 2009) was
219 used to provide the meteorological forcing for the HYSPLIT model. Variations in specific
220 humidity along the moisture trajectories were also calculated. Considering the variation in
221 boundary layer height at Kathmandu during the study period, ranging from approximately 100 m
222 to 1170 m, and with the majority of the data falling below 600 m, we set the initial starting
223 height for the moisture backward trajectories to 500 m above ground.

224 **3 Results and discussion**

225 **3.1 Isotope dynamics and their relation with local weather before, during,**
226 **and after cyclone events**

227



228

229 **Figure 2 Water vapour isotopic evolution (hourly averages) before, during, and after the**
230 **Tauktae and Yaas cyclone events as indicated by the colour shading along with associated**
231 **surface air temperature, relative humidity (RH), and rainfall amount. The blue dashed line**
232 **represents daily average.**

233 Significant variability was observed in isotopic composition before, during, and after the
234 cyclones at Kathmandu station (Figure 2 and Table 1). $\delta^{18}\text{O}_v$ and δD_v showed a sudden depletion
235 in isotopic composition at the final stages of both cyclones, coinciding with RH reaching
236 maximum values. The depletion was more pronounced during cyclone Yaas compared to
237 cyclone Tauktae.

238 Before the cyclone Tauktae, $\delta^{18}\text{O}_v$ (δD_v) varied from -7.40 ‰ (-49.53 ‰) to -12.10 ‰ (-
239 84.15 ‰) with an average of -10.04 ‰ (-69.51 ‰) and $d\text{-excess}_v$ ranged from 4.24 ‰ to 15.38
240 ‰ with an average of 10.84 ‰. The isotopic composition clearly shows a downward trend as the
241 remnant of cyclones passed over Kathmandu. $\delta^{18}\text{O}_v$ decreased by over 12 ‰ from 14 May to 20
242 May (Tauktae) and again between 24 May and 29 May (Yaas), reaching minima for $\delta^{18}\text{O}_v$ (δD_v)
243 of -20.21 ‰ (-149.49 ‰) and -24.92 ‰ (-183.34 ‰), respectively. During Tauktae, $\delta^{18}\text{O}_v$ (δD_v)
244 varied from -8.20‰ (-56.06‰) to -20.21‰ (-149.49‰) with an average of -14.73‰ (-106.76‰)
245 and during Yaas the range was from -12.17‰ (-83.85‰) to -24.92‰ (-183.34‰) with an
246 average of -17.87‰ (-129.18‰). Similarly, $d\text{-excess}_v$ during Tauktae varied from 7.97 ‰ to
247 14.24 ‰ with an average of 11.06 ‰ while during Yaas it varied from 8.71 ‰ to 18.29 ‰ with
248 an average of 13.77 ‰. After both cyclones had dissipated, $\delta^{18}\text{O}_v$ (and δD_v) started to recover
249 pre-cyclone values of -8.29 ‰ to -14.94 ‰ (-57.40 ‰ to -109.31 ‰), with an average of -11.09
250 ‰ (-79.38 ‰), and a $d\text{-excess}$ ranged between 1.80 ‰ and 15.11 ‰ with an average of 9.37 ‰.

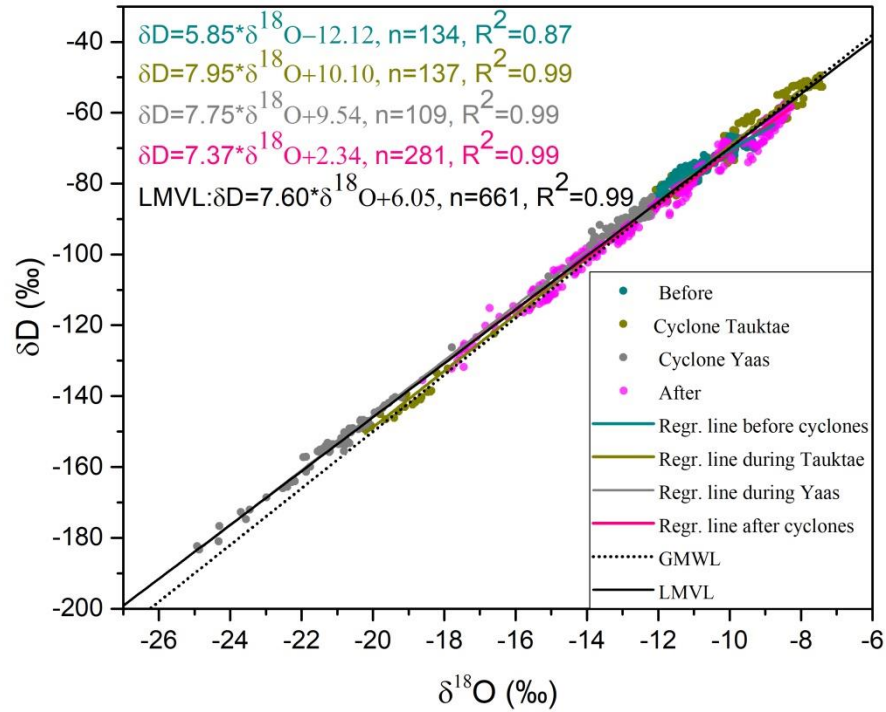
251 The remnants of cyclone Tauktae caused light rain at Kathmandu, with a significant
252 depletion in $\delta^{18}\text{O}_v$ (δD_v) by ~ 8 ‰ (~ 66 ‰) on 20 May compared to the previous day. From the
253 formation of a depression over the AS on 14 May 2021 until the dissipation inland on 19 May ,
254 no significant variation in the isotopic composition in atmospheric water vapour at Kathmandu
255 was observed (Fig. 2). After the dissipation, when the residual Tauktae vapour passed the
256 Kathmandu site producing light rains, $\delta^{18}\text{O}_v$ and δD_v began to decrease independently of the
257 rainfall amount, starting on 19 May around 11:00 h Local Time (LT), from -8.34 ‰ for $\delta^{18}\text{O}_v$
258 and -56.06 ‰ for δD_v and decreasing in one hour to -10.12 ‰ and -68.41 ‰ respectively. This
259 decrease continued for 24 hours reaching a minimum of -20.21 ‰ and -149.49 ‰ for $\delta^{18}\text{O}_v$ and
260 δD_v respectively on 20 May at 12:00 h LT. However, $d\text{-excess}_v$ did not show notable variations
261 during the passage of cyclone Tauktae. $\delta^{18}\text{O}_v$ and δD_v remained depleted from 20 to 22 May.

262 On 24 May, cyclone Yaas formed over the BoB and followed a trajectory through north-
263 eastern India. The effect of cyclone Yaas on $\delta^{18}\text{O}_v$ and δD_v at Kathmandu was observed on 25
264 May with $\delta^{18}\text{O}_v$ (δD_v) dropping rapidly from -12.62 ‰ (-88.71 ‰) on 25 May at 20:00 h LT to -
265 15.07 ‰ (-106.22 ‰) just one hour later. At the same time, $d\text{-excess}_v$ increased from 12.30 ‰ to
266 14.34 ‰. The depletion continued until 28 May with a minimum of $\delta^{18}\text{O}_v$ (δD_v) by -24.92 ‰ (-
267 182.35 ‰) at 16:00 h LT. Yaas had already weakened into a low-pressure area over Bihar in
268 south-eastern Uttar Pradesh, India. $\delta^{18}\text{O}_v$ and δD_v started to increase by about 10 ‰ on 29 May
269 at 16:00 h LT after Yaas had dissipated. From 25 to 29 May, $d\text{-excess}_v$ gradually increased as
270 opposed to $\delta^{18}\text{O}_v$ and δD_v , resulting in a negative correlation with $\delta^{18}\text{O}_v$ and δD_v of -0.60 and -
271 0.55 respectively.

272 The passage of cyclones that had formed over the AS (Tauktae) and BoB (Yaas) caused
273 significant depletion in the isotopic composition and led to cumulative rainfall of 9.2 mm

274 (Tauktae) between 14 May and 20 May 2021 and 59.6 mm (Yaas) between 25 May and 28 May
275 2021 at our site. This depletion is due to cyclone-associated intense rainfall and agrees with
276 previous studies (Krishnamurthy and Shukla, 2007; Rahul et al., 2016). Note the above $\delta^{18}\text{O}_v$
277 minimum (-24.92 ‰) observed during cyclone Yaas is similar to the minima observed in
278 Bangalore, India ($\delta^{18}\text{O}_v = -22.5$ ‰) (Rahul et al., 2016) and Roorkee, India ($\delta^{18}\text{O}_v = -25.35$ ‰)
279 (Saranya et al., 2018) when cyclones evolved over the BoB passed near their sampling sites.
280 These results indicate a similar oceanic source of moisture during cyclones. We discuss the
281 influence of moisture sources in Sect. 3.2.

282 The relation between $\delta^{18}\text{O}_v$ and δD_v varies for the periods before, during, and after the
283 cyclones, showing different slopes and intercepts with the Local Meteoric Vapour Line (LMVL)
284 (Figure 3). Before the first event, both the slope (5.85) and intercept (-12.12) are significantly
285 lower indicating the strong influence of non-equilibrium processes such as evaporation. During
286 both cyclones the slopes and intercepts resemble those of the global meteoric water line
287 (GMWL: $\delta\text{D} = 8 \times \delta^{18}\text{O} + 10$) (Figure 3). After the cyclones, the slope and intercept decreased to
288 7.37 and 2.34 respectively, implying a change of moisture sources and evaporation.



289

290 **Figure 3 Relationships between $\delta^{18}\text{O}_v$ and δD_v before, during, and after the cyclone events.**

291 **The regression lines for each period are presented along with GMWL for comparison.**

292 **Table 1 Descriptive statistics of $\delta^{18}\text{O}_v$, δD_v , and d-excess_v measured before, during, and**

293 **after the cyclone events.**

Period	$\delta^{18}\text{O}_v$ [‰]			δD_v [‰]			d-excess _v [‰]		
	min	max	avg	min	max	avg	min	max	avg
Before	-12.10	-7.40	-10.04	-84.15	-49.53	-69.51	4.24	15.38	10.84
Cyclone Tauktae	-20.21	-8.20	-14.73	-149.49	-56.06	-106.76	7.97	14.24	11.06
Cyclone Yaas	-24.92	-12.17	-17.87	-183.34	-83.85	-129.18	8.71	18.29	13.77
After	-14.94	-8.29	-11.09	-109.31	-57.40	-79.38	1.80	15.11	9.37

294

295 To assess the meteorological influence on the isotopic composition at Kathmandu, we
296 examined the linear correlations between the isotopic composition ($\delta^{18}\text{O}_v$, δD_v , and d-excess_v),
297 and air temperature (T), relative humidity (RH), precipitation amount (P), wind speed (WS), and
298 dew point temperature (T_d) before, during, and after the cyclones (Table 2). Before the cyclones,
299 both $\delta^{18}\text{O}_v$ and δD_v showed a positive correlation with air temperature (i.e., temperature effect)
300 and dew point temperature but no correlations with other meteorological variables (Table 2). The
301 correlation between $\delta^{18}\text{O}_v/\delta\text{D}_v$ and surface air temperature and RH became weaker during the
302 cyclone Tauktae while much stronger ($r=0.60$ for temperature and $r=-0.68$ for RH) during Yaas.
303 During Tauktae, we did not observe any effect of precipitation amount on the isotopic
304 composition, while during Yaas there was a negative correlation ($r=-0.56$). D-excess_v was
305 positively correlated with local air temperature (negatively correlated with local RH) before,
306 during, and after Tauktae, whilst no correlations were observed during Yaas (Table 2).

307

308

309

310

311

312

313

314

315 **Table 2 Linear correlations between the isotopic composition of atmospheric water vapour**
316 **($\delta^{18}\text{O}_v$, δD_v , and d-excess_v) and air temperature (T), relative humidity (RH), precipitation**
317 **amount (P), wind speed (WS), and dew point temperature (T_d) before, during, and after the**
318 **cyclone events. ***, **, and * indicate correlation significance levels of 0.001, 0.01, and 0.05**
319 **respectively.**

Before					
	T	RH	P	WS	T_d
$\delta^{18}\text{O}_v$	0.24 ^{***}	-0.03	-0.41	-0.10	0.51 ^{***}
δD_v	0.44 ^{***}	0.21 ^{**}	-0.37	0.08	0.63 ^{***}
d-excess _v	0.66 ^{***}	-0.64 ^{***}	0.35	0.68 ^{***}	0.28 ^{***}
Cyclone Tauktae					
$\delta^{18}\text{O}_v$	0.15	-0.19	0.11	-0.004	0.07
δD_v	0.21 [*]	-0.25 ^{**}	0.10	0.05	0.11
d-excess _v	0.77 ^{***}	-0.82 ^{***}	-0.22	0.61 ^{***}	0.51 ^{***}
Cyclone Yaas					
$\delta^{18}\text{O}_v$	0.60 ^{***}	-0.68 ^{***}	-0.56 ^{***}	0.02	0.23 ^{**}
δD_v	0.63 ^{***}	-0.70 ^{***}	-0.56 ^{***}	0.05	0.26 ^{**}
d-excess _v	0.10	-0.006	0.19	0.32 ^{**}	0.26 [*]
After					
$\delta^{18}\text{O}_v$	0.17 [*]	-0.19 [*]	-	0.19 [*]	0.09
δD_v	0.30 ^{***}	-0.31 ^{***}	-	0.30 ^{***}	0.20 [*]
d-excess _v	0.62 ^{***}	-0.58 ^{***}	-	0.52 ^{***}	0.55 ^{***}

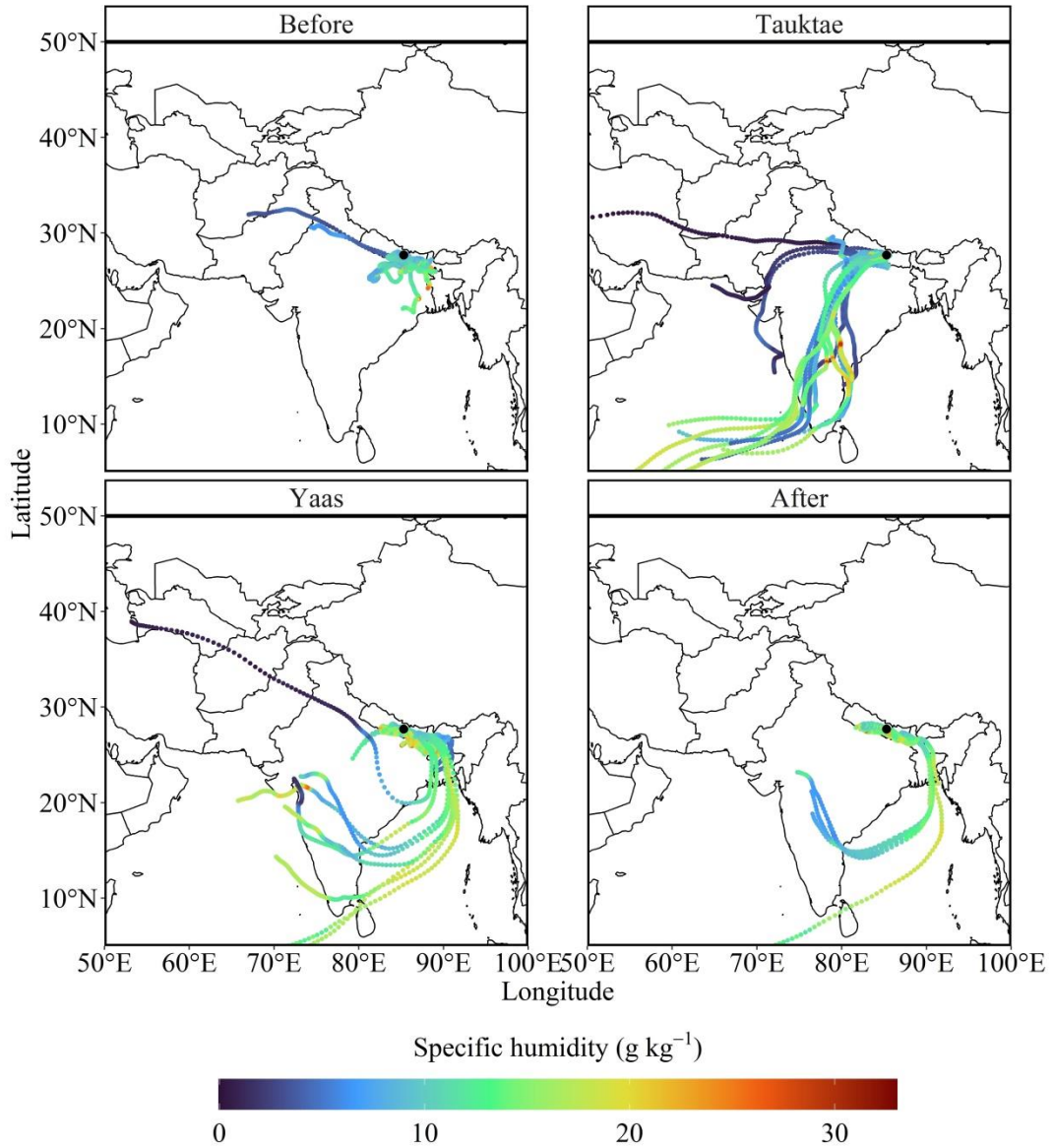
320

321 **3.2 Influence of moisture source**

322 Previous studies suggested that Kathmandu is predominantly impacted by local moisture
323 sources with short and long-range transport of westerlies before the onset of summer monsoon,
324 which is generally dry and characterized by sporadic rainfall with enriched $\delta^{18}\text{O}$ values in
325 precipitation (Adhikari et al., 2020; Chhetri et al., 2014; Yu et al., 2016). We found significant
326 proportions of moisture trajectories prior to cyclone Tauktae either originated locally or by
327 westerlies, characterized by low specific humidity (Fig. 4, upper left panel). These moisture
328 trajectories were traced back to the Gangetic plain before cyclone Tauktae. The associated $\delta^{18}\text{O}_v$

329 and δD_v values for these moisture sources exhibited enrichment, with average values of -10.04‰
330 and -69.51‰ for $\delta^{18}O_v$ and δD_v , respectively. A similar slope (5.85) and intercept (-12.12) of the
331 local meteoric vapour line before Tauktae to the surface water line calculated in the Gangetic
332 plain (Hassenruck - Gudipati et al., 2023) which provided corroboration for the impact of local
333 evaporation on the isotopic composition.

334 As cyclone Tauktae approached the continent, the primary moisture to Kathmandu was
335 coming from the Arabian Sea, instead of local origins (Fig. 4, upper right panel). The specific
336 humidity along these trajectories exhibited higher levels over the oceans, diminishing as they
337 traversed over land through precipitation (Fig. 4, upper right panel). During this phase, $\delta^{18}O_v$ and
338 δD_v were significantly lower (on average over 4.5‰ and 37‰ for $\delta^{18}O_v$ and δD_v respectively)
339 than measurements preceding the cyclone. Such depletion can be attributed to the progressive
340 rainout along the moisture transport path, wherein heavy isotopes are removed during successive
341 condensation (Xu et al., 2019). Notably, the isotopic composition before the Tauktae-induced
342 rainfall remained enriched, reflecting inflow from the surface layer (Munksgaard et al., 2015).
343 Furthermore, the $d\text{-excess}_v$ variation at Kathmandu during Tauktae may have been influenced by
344 local moisture recycling processes.



345

346 **Figure 4 Five-day backward trajectories reaching the sampling site before, during, and**
 347 **after the cyclone events. Colours denote specific humidity (q in g kg^{-1}) along the**
 348 **trajectories.**

349 During cyclone Yaas, only the BoB vapour contributed to moisture at Kathmandu and
 350 specific humidity along the trajectories over the ocean was high (Fig. 4, bottom left panel). The
 351 high specific humidity over India and surrounding regions during cyclone formation suggest that

352 Yaas lifted a substantial amount of water vapour from the BoB yielding intense rainfall along its
353 path. The isotopic composition during Yaas was more depleted than that of Tauktae with
354 averages of -17.87‰ and -129.18‰ for $\delta^{18}\text{O}_v$ and δD_v respectively. The difference could stem
355 from varied moisture sources, rainout histories, and the respective strengths of each cyclone.
356 Moreover, the high isotopic depletion during cyclone Yaas might be attributed to the disparity of
357 sea surface water $\delta^{18}\text{O}$ between the AS and BoB. The surface water $\delta^{18}\text{O}$ in the BoB is relatively
358 depleted compared to the AS (Lekshmy et al., 2014), which results from a substantial influx of
359 freshwater from rain and runoff originating from the Ganga Brahmaputra river basin
360 (Breitenbach et al., 2010; Singh et al., 2010).

361 Although, the progressive increment was seen in the time series of $\delta^{18}\text{O}_v$ and δD_v after
362 the dissipation of Tauktae (Fig. 2), $\delta^{18}\text{O}_v$ and δD_v in the earlier stage of Yaas were significantly
363 lower compared to Tauktae because there was not enough time for recovery. There was a strong
364 association between $\delta^{18}\text{O}_v$ /or δD_v and local meteorological conditions during cyclone Yaas
365 associated with high relative humidity from the remote ocean (Chen et al., 2021; Xu et al., 2019).
366 Furthermore, the negative correlation of $\delta^{18}\text{O}_v/\delta\text{D}_v$ vs. RH and the fact that $\delta^{18}\text{O}_v/\delta\text{D}_v$ was
367 depleted highlight the influence of humid moisture sources (Yu et al., 2008), which was also
368 confirmed by our moisture backward trajectory analysis (Fig. 4, bottom left panel). A similar
369 correlation was also observed in mid-tropospheric water vapour over the western Pacific
370 associated with intense convective activity (Noone, 2012).

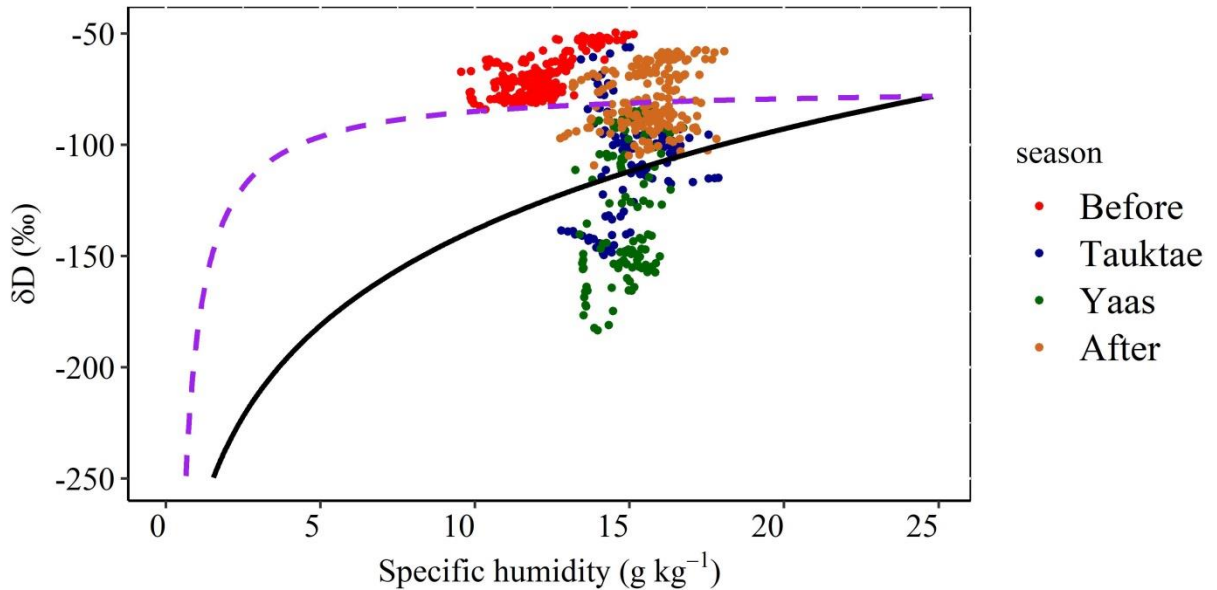
371 In contrast to cyclone Tauktae, the lack of correlation of $d\text{-excess}_v$ with RH and local air
372 temperature during cyclone Yaas implies that local moisture recycling processes are not
373 significant in determining $d\text{-excess}_v$ variation and RH might not be a reliable predictor of kinetic
374 fractionation during evaporation. Previous research conducted in the Indian Ocean (e.g., Midhun

375 et al., 2013; Uemura et al., 2008) suggested that the high relative humidity (i.e. >80%) at the
376 sampling sites weakens the correlation between $d\text{-excess}_v$ and RH. Our observed data also
377 satisfied that condition during Yaas because the majority of isotopic measurements (about 75%)
378 were associated with high relative humidity (>80%), while this fraction was only 25% during
379 Tauktae.

380 Following the dissipation of the cyclones, some portion of moisture at Kathmandu was
381 provided by BoB source together with local evaporation (Fig. 4, bottom right panel). However,
382 the isotopic composition reverted to the original (enriched) levels ($\delta^{18}\text{O}_v = -11.09 \text{ ‰}$, $\delta\text{D}_v = -$
383 79.38 ‰ , and $d\text{-excess}_v = 9.37 \text{ ‰}$). The diminished correlation between $\delta^{18}\text{O}_v/\delta\text{D}_v$ and
384 temperature following the cyclones is attributed to the admixture of vapour originating from
385 plant transpiration during that period (Delattre et al., 2015).

386 We used the vapour $\delta\text{D}_v\text{-}q$ plot combined with the Rayleigh distillation and mixing curve
387 to assess the moisture mixing (Fig. 5). Before the development of cyclone Tauktae and during its
388 early stages, the data points lie well above the mixing curve, indicating that the isotopic
389 variability was mainly dominated by vapour from local evapotranspiration. In contrast, during
390 the latter stage of cyclone Tauktae, δD_v was significantly depleted to levels well below the
391 Rayleigh curve. During the early stage of cyclone Yaas, there are only a few data points between
392 the mixing and Rayleigh curves with the majority well below the Rayleigh curve, particularly
393 during the later stage. During both events, Kathmandu was dominated by deep convection
394 leading to a strong convergence of moisture from both the AS (Tauktae) and the BoB (Yaas).
395 This points towards the influence of convective processes (see Section 3.3) (Galewsky and
396 Samuels-Crow, 2015). After Yaas had dissipated, δD_v gradually increased again with half of the
397 data points clustered between the mixing and Rayleigh curves. The remaining data points were

398 well above the mixing curve, indicating the influence of locally evaporated vapour also
399 evidenced by the moisture back trajectories (**Error! Reference source not found.** bottom right
400 panel).



401
402 **Figure 5** Scatter plot of hourly averaged δD_v vs. specific humidity (q). The solid black curve
403 represents the Rayleigh distillation curve calculated for the initial condition of $\delta D_v = -78.20$
404 ‰, BoB-averaged δD_v (Lekshmy et al., 2022), SST of 30°C , and RH of 90 %. The dashed
405 purple curve represents the mixing line, calculated based on dry continental air ($q = 0.5 \text{ g kg}^{-1}$
406 and $\delta D_v = -300 \text{ ‰}$ (Wang et al., 2021)) and the wet source, which corresponds to the
407 **initial conditions used to calculate the theoretical Rayleigh curve.**

408 **3.3 Influence of deep convection associated with cyclones**

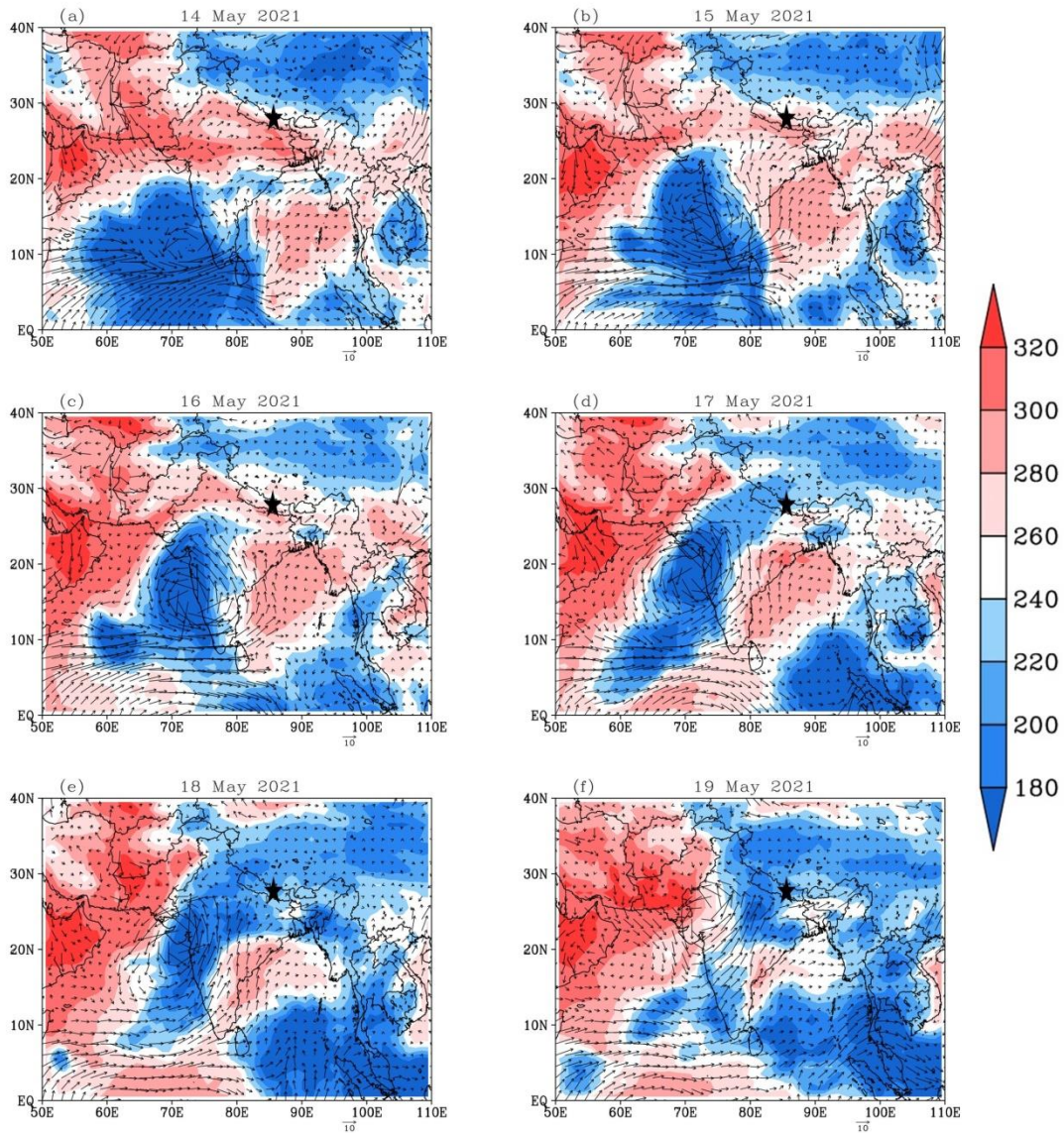
409 One of the likely causes for large isotopic depletion during cyclones might be the
410 associated convective processes. Studies have demonstrated that convective processes within
411 tropical cyclones can cause the depleted isotopic composition of precipitation and atmospheric
412 water vapour (Fudeyasu et al., 2008; Jackisch et al., 2022; Munksgaard et al., 2015) due to a

413 combination of strong cyclonic circulation, intense large-scale convection, heavy precipitation,
414 and high wind speeds (Chen et al., 2021; Xu et al., 2019). We analysed the relationship between
415 the isotopic composition and convective processes, using OLR and vertical velocity as a proxy
416 for convection. Due to the frequent co-occurrence of intense convection and significant mid-
417 tropospheric convergence of moist air, the vertical velocities can also serve as a proxy for
418 convective activity (Lekshmy et al., 2014).

419 Figure 6 and Figure 7 depict the prevalence of strong convective processes associated
420 with both cyclones throughout their lifespan. During the initial days of cyclone formation, OLR
421 exceeded 260 Wm^{-2} in the area of the sampling site and decreased rapidly to below 200 Wm^{-2} in
422 the final stages of both cyclones when approaching the site. Although the amount of precipitation
423 associated with Tauktae (9.2 mm) was much lower than Yaas (59.6 mm), $\delta^{18}\text{O}_v$ depleted by up to
424 12 ‰ during both cyclones. The progressive rainout was evident along the entire cyclone track
425 (Figs. S4 and S5), and the spatial distribution of precipitation was highly correlated with the
426 convective process suggesting rainfall occurred from the deep convective cloud rather than local
427 evaporation. This was confirmed by precipitation variations. The site received its first rainfall on
428 19 May during cyclone Tauktae and on 25 May during cyclone Yaas, as shown in Figure S4 and
429 Figure S5. *In situ* observations confirm that during the days leading up to cyclone Tauktae, the
430 sampling site received a total of 12.2 mm of precipitation with maximum rainfall of 9.2 mm/h
431 recorded on 11 May at 13:00 h LT, equal to the total accumulated rainfall during the entire
432 cyclone. Although the pre and during-Tauktae rainfall amounts are similar, pre-cyclone $\delta^{18}\text{O}_v$
433 and δD_v were significantly more enriched (averages: $\delta^{18}\text{O}_v = -10.04 \text{ ‰}$ and $\delta\text{D}_v = -69.51 \text{ ‰}$)
434 than during Tauktae (averages: $\delta^{18}\text{O}_v = -14.73 \text{ ‰}$ and $\delta\text{D}_v = -106.76 \text{ ‰}$). We compared the
435 values of $\delta^{18}\text{O}_v$, δD_v , and $d\text{-excess}_v$ during both events and also examined them in comparison

436 with the isotopic composition at the beginning of the summer monsoon (June 2021). This initial
437 period of intense and continuous rainfall at our sampling site (Fig. S6) is regulated by the
438 monsoon system originating in the BoB. Consequently, our focus centered on the isotopic
439 distinctions between water vapour on typical rainy days and that associated with cyclone Yaas.

440



441

442 **Figure 6 Regional winds (arrows) and outgoing longwave radiation (colours in Wm^{-2})**

443

during cyclone Tauktae.

444 Following the initiation of the summer monsoon, both $\delta^{18}\text{O}_v$ and δD_v exhibited a

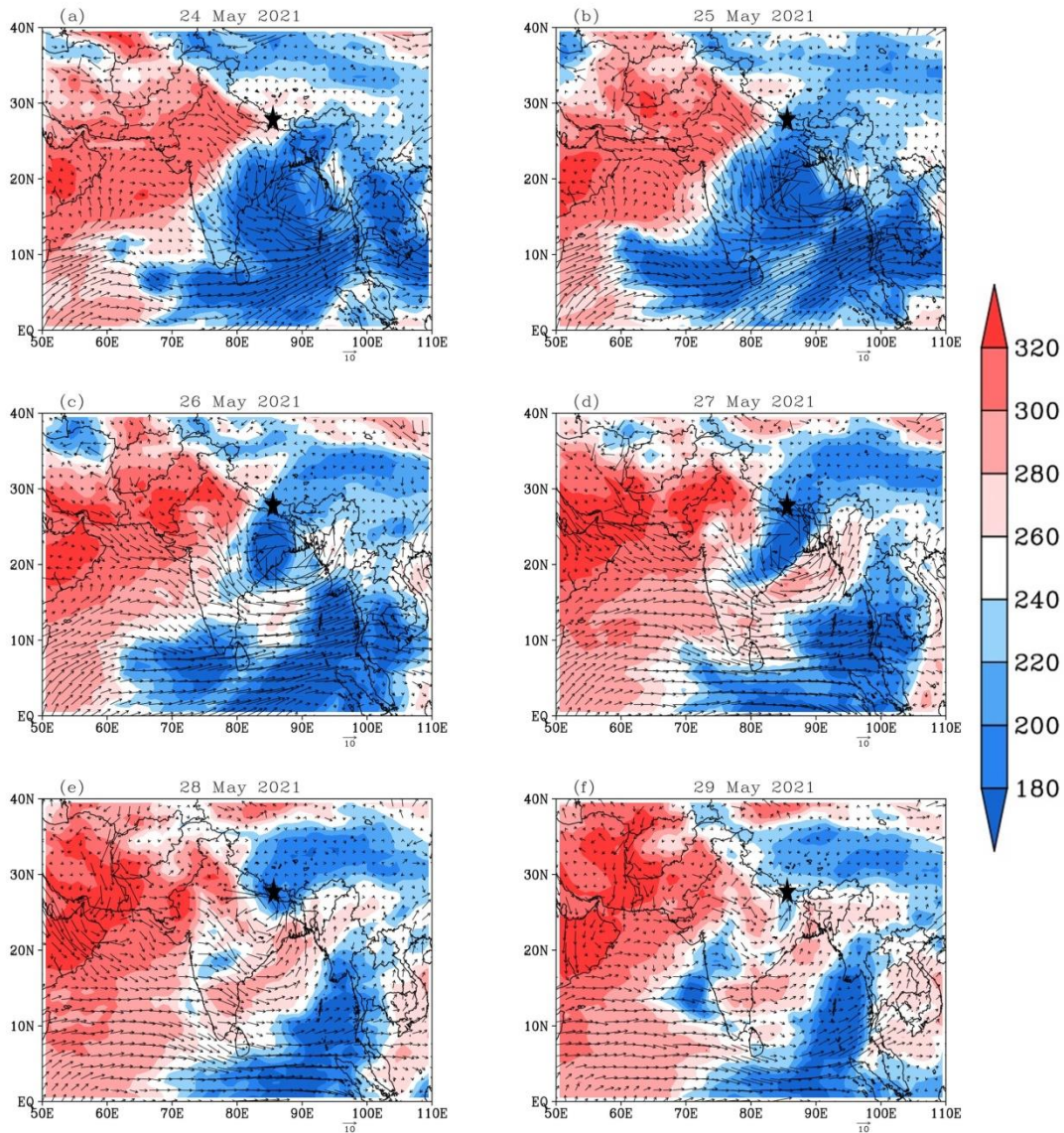
445 progressive depletion, coinciding with a decline in air temperature, an increase in relative

446 humidity (RH), and amplified rainfall amounts (Fig. S6). Despite the daily accumulated rainfall

447 and RH being significantly higher during the normal monsoon period, both $\delta^{18}\text{O}_v$ and δD_v were

448 markedly lower during cyclone Yaas (on average by over 2.5‰ and 26‰ for $\delta^{18}\text{O}_v$ and δD_v

449 respectively) compared to typical rainy days. A progressive reduction in $d\text{-excess}_v$ was also
450 evident as the summer monsoon unfolded; a trend typically observed in precipitation d-excess
451 (e.g., Hussain et al., 2015; Acharya et al., 2020; Adhikari et al., 2020) and water vapour d-excess
452 (Tian et al., 2020; Yao et al., 2018; He and Richards, 2016; Wei et al., 2016) in Asian monsoon
453 regions, in contrast to our observations during cyclone Yaas.



454

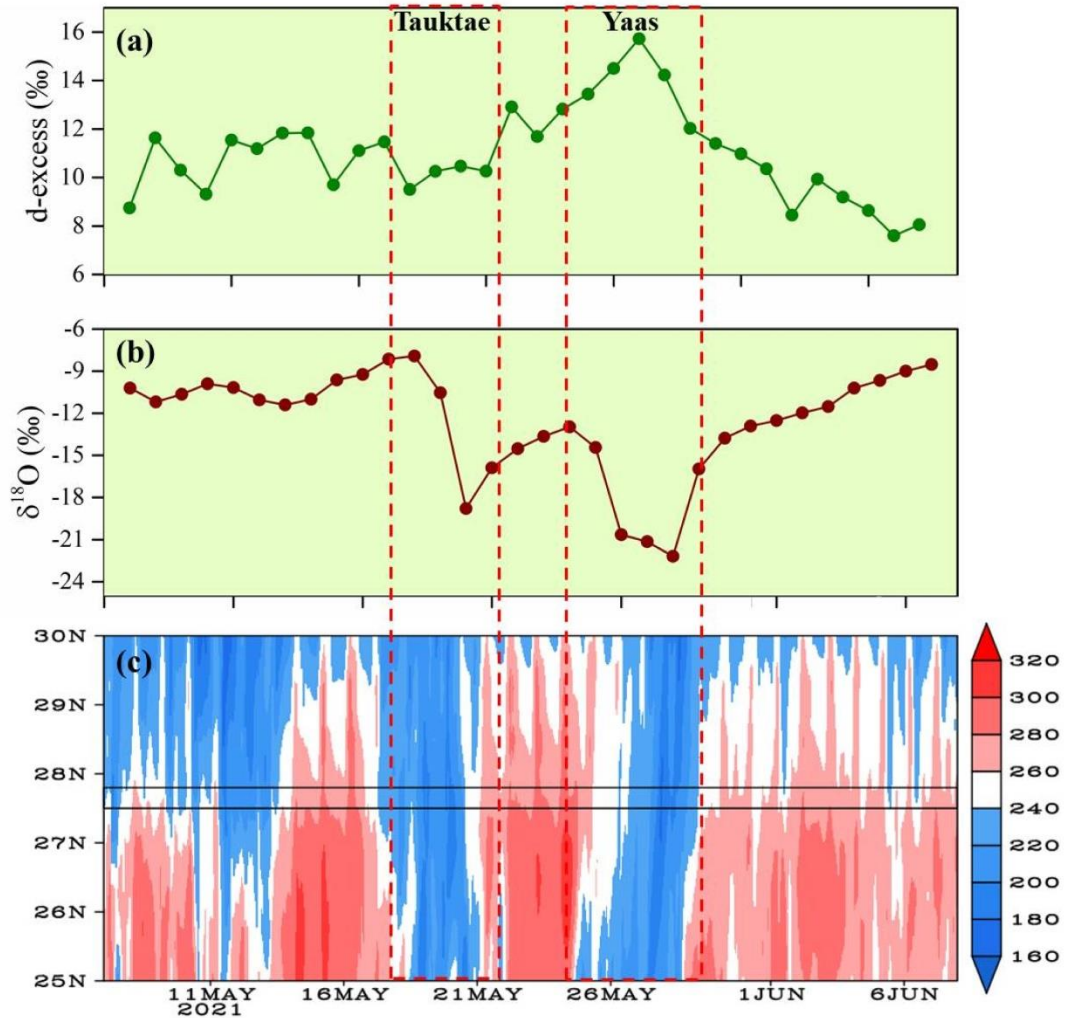
455

Figure 7 Same as Figure 6 but for cyclone Yaas.

456 Given that d-excess has long served as a diagnostic tool for understanding moisture
457 source conditions (Tian et al., 2001; Liu et al., 2008), the distinct behaviour of d-excess_v between
458 cyclone Yaas and the normal monsoon phase suggests that cyclone-related information may be
459 discerned through the isotopic composition recorded at our site. This confirms our previously
460 stated hypothesis that rainfall associated with cyclones causes significantly lower isotope values
461 in vapour due to intense convective systems (Gedzelman et al., 2003; Kurita, 2013), absent in
462 local rain events and days without precipitation (Lekshmy et al., 2022).

463 The influence of convective processes on water vapour isotopic variations at Kathmandu
464 is further supported by the Hovmöller diagram of OLR averaged over 80-90° E, which clearly
465 shows that $\delta^{18}\text{O}_v$ depletion coincides with the presence of clouds (Figure 88b and c). In contrast,
466 d-excess_v showed dissimilar variations between both cyclones. Before cyclone Tauktae, the daily
467 averaged d-excess_v was above the global average of 10 ‰ (Fig. 8a). Once Tauktae approached
468 our sampling site, d-excess_v decreased from around 12 ‰ to 10 ‰ and continued to oscillate
469 about 10 ‰ until Tauktae had dissipated. As cyclone Yaas approached the measurement site
470 with intense rainfall (Fig. 2), d-excess_v gradually increased while RH increased and air
471 temperature decreased (Fig. 2). Specifically, d-excess_v on 24 May was recorded as 12.82 ‰
472 when surface air temperature and surface RH was about 24 °C and 70 % respectively. On 27
473 May, we noted a 3 ‰ rise in d-excess_v when the surface temperature was reduced by 4 °C and the
474 surface RH was increased by 19 %. The combination of increasing d-excess and decreasing
475 $\delta^{18}\text{O}_v$ highlights the role of vapour recycling due to the subsidence of air masses from stratiform
476 clouds (Kurita et al., 2011). In addition, a large increase in d-excess_v was also recorded in
477 atmospheric vapour during cyclone Ita in 2014 and was attributed to downward moisture
478 transport above the boundary layer (Munksgaard et al., 2015). We did not find any statistically

479 significant correlation during cyclone Yaas between $d\text{-excess}_v$ and RH/Temperature, although
480 RH is considered an important parameter for interpreting $d\text{-excess}$ in atmospheric vapour and
481 precipitation (Pfahl and Sodemann, 2014; Steen-Larsen et al., 2014). The observed co-
482 occurrence of higher $d\text{-excess}_v$, lower temperatures, and high relative humidity (Fig. 2) points to
483 kinetic fractionation processes either at a larger scale or in association with downdrafts (Conroy
484 et al., 2016). Rain re-evaporation under the condition of high saturation deficit is one of the
485 causes of low $\delta^{18}\text{O}_v$ and high $d\text{-excess}_v$. This is due to the addition of re-evaporated vapour
486 during precipitation events, which results in depleted cloud vapour and high $d\text{-excess}_v$ (Conroy et
487 al., 2016; Lekshmy et al., 2014). On normal days high $d\text{-excess}_v$ values were generally
488 accompanied by low RH (**Error! Reference source not found.S7**) and vice versa. However, the
489 high relative humidity of the surface air together with near saturation conditions vertically
490 (Figure 99b) during cyclone Yaas, rule out any effect of re-evaporation on increased $d\text{-excess}_v$
491 values. Such high $d\text{-excess}_v$ values may be associated with downdrafts during convective rain
492 events, transporting isotopically depleted vapour with higher $d\text{-excess}_v$ values from the boundary
493 layer to the surface (Kurita, 2013; Midhun et al., 2013).



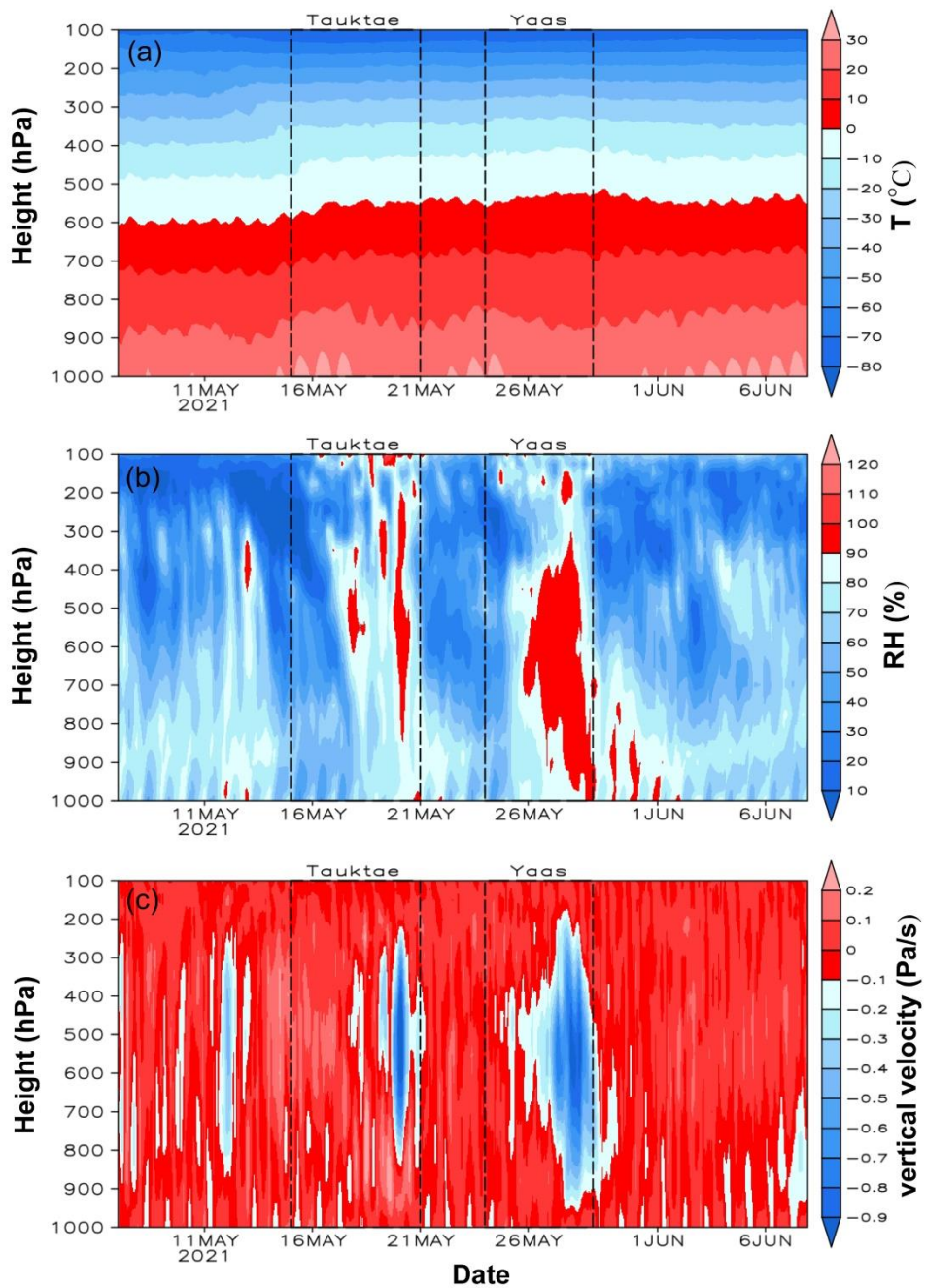
494

495 **Figure 8** Time series of daily averaged $d\text{-excess}_v$ (a), $\delta^{18}\text{O}_v$ (b), and Hovmöller diagram of
 496 **OLR (Wm^{-2}) averaged over $80^\circ \text{E}-90^\circ \text{E}$ (c) The solid parallel lines in (c) depict the latitude**
 497 **range of sampling site.**

498 To clarify the impact of convection on the isotopic composition, we analysed the
 499 distribution of vertical velocity, relative humidity, and air temperature averaged over a box
 500 between $25^\circ\text{N}-28^\circ\text{N}$ and $83^\circ\text{E}-87^\circ\text{E}$ with our measurement site near its center (Fig. 9). Our
 501 results show that strong shifts in $\delta^{18}\text{O}_v$, δD_v , and $d\text{-excess}_v$ during the cyclones were strongly
 502 associated with vertical air motions (Figure 99c). We observed a general downward movement

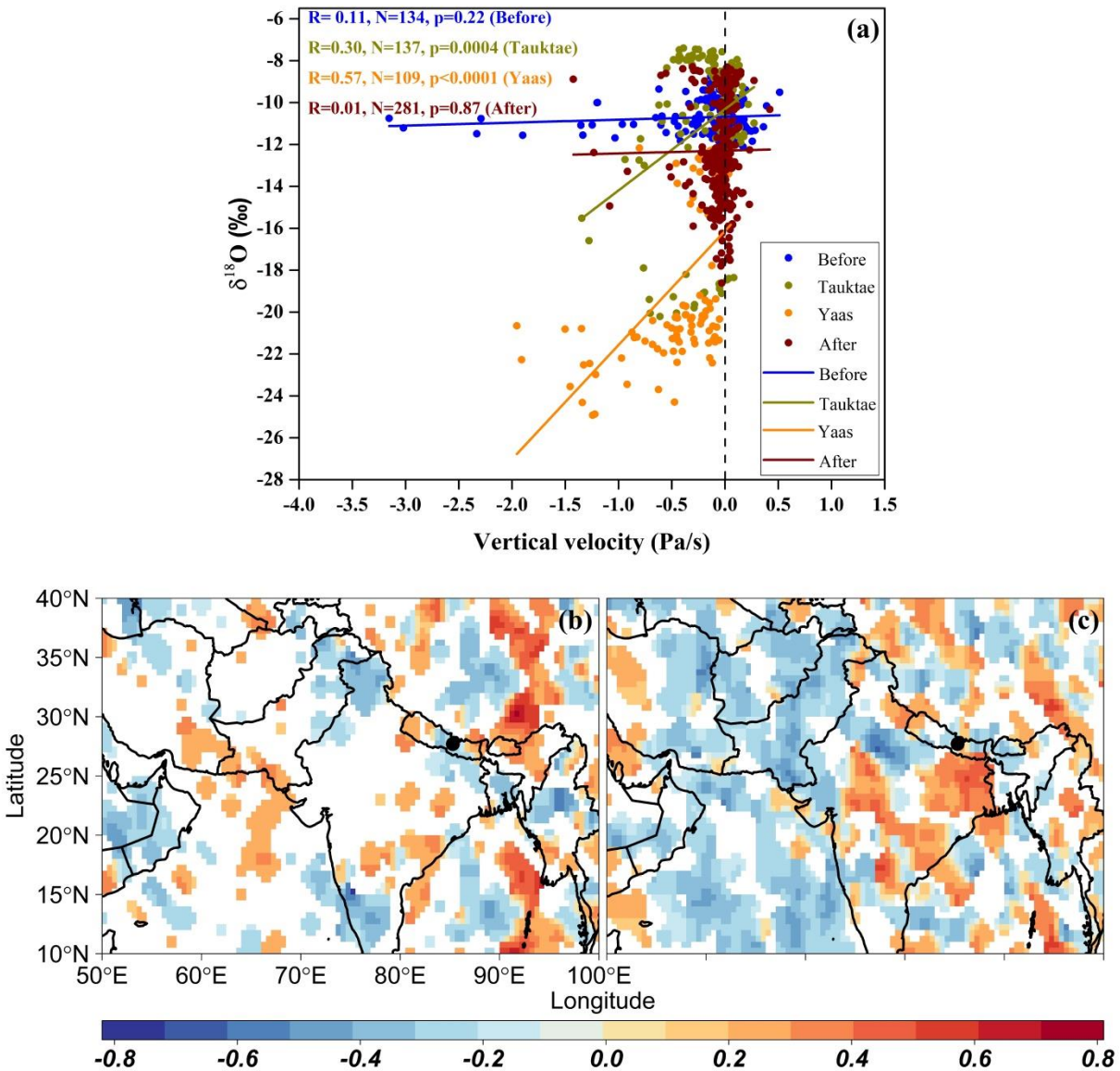
503 of air before the rain started with Tauktae. The high depletion of $\delta^{18}\text{O}_v$ and δD_v during the final
504 stages of Tauktae (Fig. 2) was accompanied by strong upward air movement extending from 800
505 hPa to about 200 hPa (Figure 9c). This upward motion was even stronger during cyclone Yaas
506 and became evident near the measurement site once Yaas made landfall on 26 May.
507 Interestingly, variations in RH at different pressure levels strongly coincided with changes in
508 vertical velocity while the lower troposphere remained near saturation (RH= ~100 %) during the
509 final stages of both cyclones (Fig. 9b). While the air temperature showed the expected decline
510 with altitude (Fig. 9a), there were no significant temporal variations during the entire period,
511 despite the high variation in RH. The strong convective updraft added additional moisture from
512 the warm ocean below, before passing over our measurement site (Lekshmy et al., 2014).
513 Convective updrafts cause moisture to condense quickly and this high-efficiency condensation of
514 heavy rain can result in more depleted $\delta^{18}\text{O}_v$ and δD_v (Lawrence and Gedzelman, 1996). In
515 addition, we found a strong positive correlation between $\delta^{18}\text{O}_v$ and average vertical velocity
516 ($r=0.57$) during Yaas at pressure levels between 300 hPa and 600 hPa (Fig. 10a) in the area
517 surrounding our site. This correlation was weaker ($r=0.30$) during Tauktae. The distinctive
518 relationship between $\delta^{18}\text{O}_v$ and vertical velocity implies that convective processes play a more
519 significant role during Yaas than Tauktae. This result was further supported by the spatial
520 distribution of correlation coefficient between $\delta^{18}\text{O}_v$ and vertical velocity (Fig. 10b, c). During
521 cyclone Tauktae, a significant negative correlation was observed between $\delta^{18}\text{O}_v$ and vertical
522 velocity around the sampling site, while positive correlation areas were identified in western
523 Nepal, certain parts of central India, and the coastal region of the Bay of Bengal (BoB) (Fig.
524 10b). A comparison with back trajectories unveiled positive correlation only in specific sections
525 along the moisture transport path, suggesting that convective processes may not be the primary

526 driver of isotopic depletion during cyclone Tauktae. Conversely, a positive correlation was
527 evident in the coastal BoB, extending north toward the sampling site during cyclone Yaas (Fig.
528 10c). The positive correlation areas were considerably larger compared to Tauktae, and these
529 areas closely aligned with the moisture transport path. Hence, higher depletion in $\delta^{18}\text{O}_v$ and δD_v
530 during Yaas, relative to Tauktae, may be attributed to the stronger convection associated with
531 BoB vapour compared to the AS vapour. The BoB is a convectively active region, and previous
532 studies reported greater depletions in $\delta^{18}\text{O}$ and δD in precipitation, irrespective of the season
533 (Breitenbach et al., 2010; Lekshmy et al., 2015; Midhun et al., 2018). Another reason we
534 observed different levels of isotope depletion between both cyclones may be related to
535 differences in their proximity to the sampling site. While Yaas came as close as 330 km to our
536 site, Tauktae was about 1050 km away when it dissipated (Fig. S8). The proximity of Yaas may
537 explain the stronger rainfall during that event which enhanced the isotopic fractionation in turn
538 leading to stronger isotopic depletion (Jackisch et al., 2022). Similar results have been
539 documented for precipitation stable isotopes (e.g., Fudeyasu et al., 2008; Jackisch et al., 2022;
540 Munksgaard et al., 2015; Xu et al., 2019) and water vapour stable isotopes (e.g., Munksgaard et
541 al., 2015; Rahul et al., 2016; Saranya et al., 2018). Even after both cyclones had dissipated,
542 progressive rainfall continued at our sampling site due to the presence of residual moisture from
543 the cyclones. Once these residual effects had diminished and rainfall intensity weakened, $\delta^{18}\text{O}_v$
544 and δD_v started to increase again (Fig. 2), likely due to evaporative effects (Munksgaard et al.,
545 2015; Xu et al., 2019; Jackisch et al., 2022).



546

547 **Figure 9** Time series of the vertical distribution of air temperature (a), RH (b), and vertical
 548 velocity (c) averaged over 25° N- 28° N and 83° E- 87° E with Kathmandu approximately at
 549 the centre. Negative (positive) vertical velocities indicate ascending (descending) winds.



550

551 **Figure 10 (a) Linear regression between $\delta^{18}\text{O}_v$ and the average vertical velocities at**
 552 **pressure levels between 300 hPa and 600 hPa, averaged over 25° N-28° N and 83° E-87° E**
 553 **which has our measurement site near its centre. (b) Spatial distribution of correlation**
 554 **coefficient between $\delta^{18}\text{O}_v$ and vertical velocity during Tauktae. (c) Same as (b) but during**
 555 **Yaas. The vertical black dashed line in (a) represents the threshold separating ascending**
 556 **(negative values) and descending (positive values) air motions.**

557 **3.4 Influence of rainfall**

558 The backward trajectories reveal the impact of separate air masses during cyclones
559 Tauktae and Yaas, specifically between the AS and BoB. We studied the meteorological
560 conditions along the 5-day moisture back trajectories, focusing on the upstream rainout on
561 observed isotopic depletion. During cyclone Tauktae, both $\delta^{18}\text{O}_v$ and δD_v display a strong
562 negative correlation ($r = -0.80$ and $r = -0.79$ for $\delta^{18}\text{O}_v$ and δD_v , respectively, Fig. S9) with total
563 precipitation along the moisture trajectories (i.e., upstream rainout). Moreover, a negative
564 correlation emerges between $\delta^{18}\text{O}_v/\delta\text{D}_v$ and average relative humidity (RH) along the trajectories
565 ($r = -0.69$ for $\delta^{18}\text{O}_v$ and -0.68 for δD_v), suggesting increased upstream rainout corresponds to
566 lower isotope ratios during cyclone Tauktae.

567 In addition, modelled back trajectories indicate that air masses during cyclone Tauktae
568 had a longer transport time when continuous rainout could have enhanced the isotopic depletion
569 of the residual vapour (Fig. 4, upper right panel). The upstream rainfall control could also
570 account for the delayed return of $\delta^{18}\text{O}_v$ and δD_v to more positive values following dissipation.

571 Similar observations have been documented in other regions; for example, the Chinese
572 Typhoons Haitang, Megi, and Soudelor (Xu et al., 2019), the Central American Hurricanes Irma
573 and Otto (Sánchez-Murillo et al., 2019), and Central Texas Hurricane Harvey (Sun et al., 2022)
574 all demonstrate significant negative correlations between upstream rainout and precipitation
575 $\delta^{18}\text{O}$. This suggests that upstream rainout could serve as a widely applicable control on the
576 spatiotemporal variability in tropical cyclones (Sun et al., 2022).

577 In contrast to cyclone Tauktae, neither the total rainfall nor the relative humidity (RH)
578 along the trajectories appears to exert influence on isotopic variation during cyclone Yaas.
579 Instead, a negative correlation was observed between $\delta^{18}\text{O}_v/\delta\text{D}_v$ and local rainfall amount, air

580 temperature, and RH (Table 2). This suggests that the observed isotopic depletion during cyclone
581 Yaas cannot be adequately explained by upstream rainout processes. We assume that sudden
582 changes in local meteorological conditions are a consequence of synoptic processes during the
583 cyclones. The progressive rainout during the cyclone events followed a temperature decrease
584 (Figure 2) which would result in the $\delta^{18}\text{O}_v/\delta\text{D}_v$ correlation with temperature (Delattre et al.,
585 2015). The cooling of surface air during rainfall, coupled with the isotopic equilibrium of vapour
586 with raindrops, establishes a positive correlation between $\delta^{18}\text{O}_v/\delta\text{D}_v$ and temperature (Midhun et
587 al., 2013). These conditions were favourable during cyclone Yaas because the sampling site
588 experienced consistent rainfall, along with a noticeable increase in relative humidity and a
589 decrease in temperature. This might be one of the reasons for the weaker correlation of $\delta^{18}\text{O}_v/\delta\text{D}_v$
590 with local meteorological variables during Tauktae.

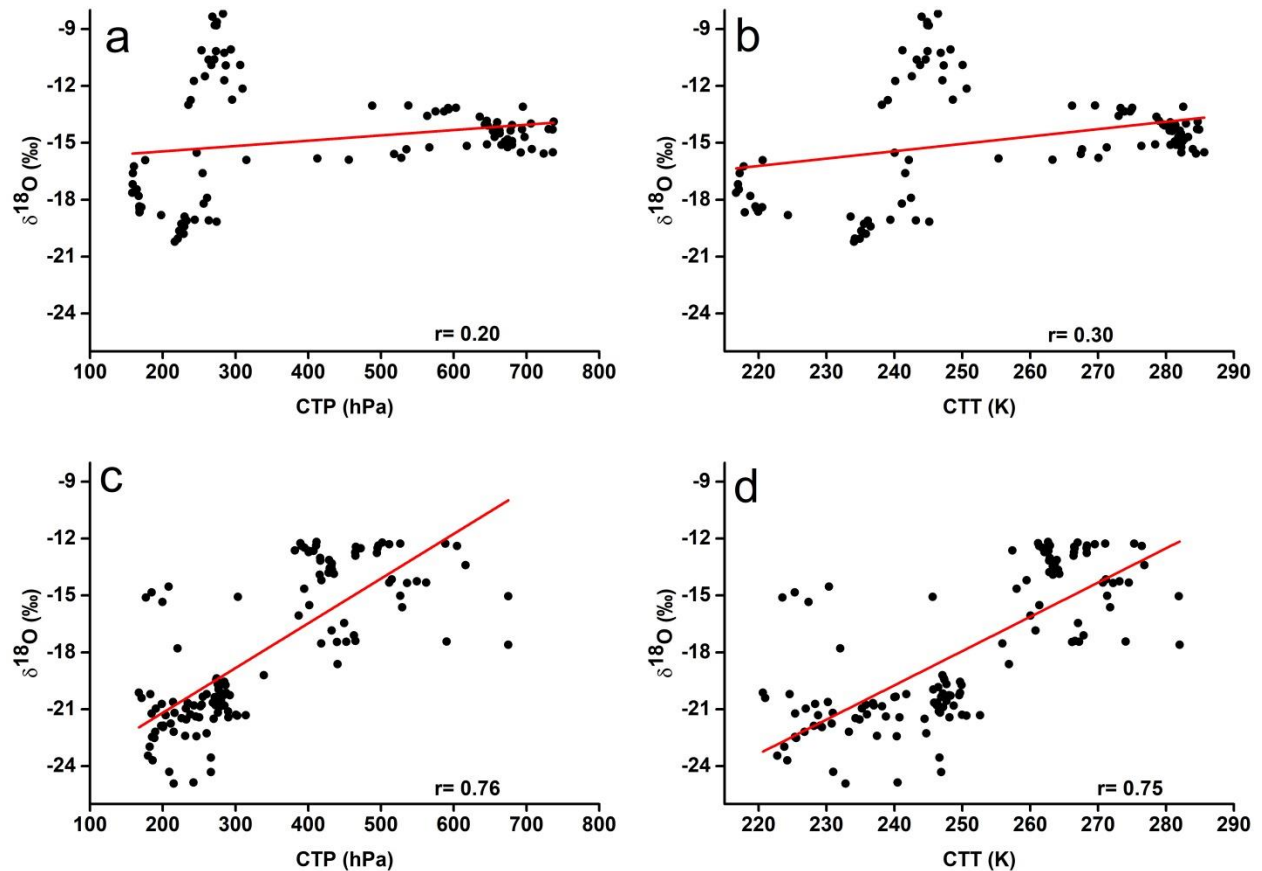
591 Studies have speculated that the impact of precipitation amount is not confined to a
592 strictly local context (Galewsky et al., 2016), but is subject to modulation by convective and
593 large-scale atmospheric properties including downdraft moisture recycling (Risi et al., 2008),
594 large-scale organized convection and associated stratiform rain (Kurita, 2013), as well as
595 regional circulation and shifting moisture sources (Lawrence et al., 2004). Our measurements
596 during cyclone Yaas revealed the presence of an intense convective system over our study site,
597 indicating that the observed effect of rainfall amount may have been governed by moisture
598 convergence (Chakraborty et al., 2016). The subsequent rainfall originating from the convective
599 system, occurring over a region characterized by depleted isotope values, resulted in a negative
600 association between precipitation amount and $\delta^{18}\text{O}_v/\delta\text{D}_v$ (Kurita, 2013). The ^{18}O -depleted water
601 vapour reaching the sub-cloud layer, accompanied by the intense convective downdrafts,

602 subsequently ascended back to the cloud level with the updrafts, in a feedback mechanism
603 proposed by Lekshmy et al., (2014).

604 **3.5 Relation with cloud-top temperature and cloud-top pressure**

605 Given that cloud-top temperature (CTT) and cloud-top pressure (CTP) are reliable
606 indicators of both moisture convergence and convective strength (Cai et al., 2018; Cai and Tian,
607 2016), we investigate the linear correlation between CTT/CTP (averaged over the 27°N-28°N
608 latitude and 85°E-86°E longitude range, with our site located at the center) and $\delta^{18}\text{O}_v$ (Fig. 11).
609 The results demonstrate a weak positive correlation between CTT/CTP and $\delta^{18}\text{O}_v$ during cyclone
610 Tauktae (Fig. 11a, b), and a robust positive correlation during cyclone Yaas (Fig. 11c, d). These
611 correlations exhibit greater strength compared to the correlation observed with local rainfall.
612 Previous research has highlighted positive correlations between $\delta^{18}\text{O}$ and CTT/CTP in the East
613 Asian Monsoon suggesting that intense convection and moisture convergence lead to an increase
614 in cloud-top height and a decrease in CTT, causing a reduction in $\delta^{18}\text{O}$ (Cai and Tian, 2016). The
615 decrease in $\delta^{18}\text{O}_v$ during cyclone Yaas coupled with a decrease in CTT and CTP (i.e. increase in
616 cloud-top height) shows the influence of intensified convective activities and moisture
617 convergence, while the isotopic depletion during cyclone Tauktae is attributed to upstream
618 rainout processes. Furthermore, a negative correlation is evident between $d\text{-excess}_v$ and
619 CTT/CTP, with $r = -0.52$ and $r = -0.60$ during cyclone Yaas. Conversely, a weak positive
620 correlation is observed during cyclone Tauktae, with $r = 0.32$ for both CTT and CTP. This
621 relationship implies that lower CTT and CTP during intense convection relate to increased $d\text{-}$
622 excess_v values during the final stage of cyclone Yaas.

623



624

625 **Figure 11 Relationship between hourly $\delta^{18}\text{O}_v$ and (a) CTT during Tauktae, (b) CTP during**
 626 **Tauktae, (c) CTT during Yaas, and (d) CTP during Yaas.**

627 **4 Conclusion**

628 This study presented the results of continuous measurements of the isotopic composition
 629 of atmospheric water vapour over Kathmandu between 7 May and 7 June 2021 covering two
 630 cyclone events; cyclone Tauktae formed over the Arabian Sea, and cyclone Yaas formed over
 631 the Bay of Bengal. $\delta^{18}\text{O}_v$ (δD_v) during Tauktae varied from -8.20‰ (-56.06‰) to -20.21‰ ($-$
 632 149.49‰) with an average of -14.73‰ (-106.76‰) and during Yaas $\delta^{18}\text{O}_v$ (δD_v) ranges from $-$
 633 12.17‰ (-83.85‰) to -24.92‰ (-183.34‰) with an average of -17.87‰ (-129.18‰). Similarly,
 634 $d\text{-excess}_v$ during Tauktae varied from 7.97‰ to 14.24‰ with an average of 11.06‰ while

635 during Yaas it varied from 8.71 ‰ to 18.29 ‰ with an average of 13.77 ‰. Both cyclones led to
636 significant depletion of $\delta^{18}\text{O}_v$ and δD_v , with $\delta^{18}\text{O}_v$ decreasing by over 12 ‰. We attribute these
637 rapid depletions to changes in moisture sources (local vs. marine) inferred from backward
638 moisture trajectories. The lower intercepts of the local meteoric vapour line before and after the
639 events highlight the influence of non-equilibrium processes such as evaporation on the isotopic
640 composition. The spatial distribution of OLR, vertical velocity, and regional precipitation during
641 both cyclonic events indicated significant moisture convergence and intense convection at and
642 around the measurement site. This resulted in depleted $\delta^{18}\text{O}_v$ and δD_v , with cyclone Yaas
643 exhibiting stronger moisture convergence and convection, leading to lower $\delta^{18}\text{O}_v$ values
644 compared to cyclone Tauktae. This difference may be attributed to robust downdrafts during
645 Yaas-related convective rain events, potentially transporting vapour with higher d-excess_v and
646 lower $\delta^{18}\text{O}_v$ values to the surface. The observed isotopic depletion during cyclone Tauktae can be
647 explained by upstream rainout processes.

648 Overall, our results show that tropical cyclones originating in the BoB and the AS during
649 the pre-monsoon season transport large amounts of isotopically depleted vapour and produce
650 moderate to heavy rainfall over a sizeable region in Nepal. The isotopic composition of
651 atmospheric water vapour and precipitation during the dry season should therefore be interpreted
652 with caution, and the effects of cyclones should not be underestimated. In addition, our results
653 underline the need for simultaneous measurements of the isotopic composition of both
654 atmospheric water vapour and precipitation to better understand post-condensation exchanges
655 between falling raindrops and boundary layer vapour over Kathmandu.

656

657 **Data Availability**

658 The data used in this study will be available in the Zenodo repository.

659 **Competing interests**

660 The contact author has declared that none of the authors has any competing interests.

661 **Acknowledgements**

662 This work was funded by ‘The Second Tibetan Plateau Scientific Expedition and
663 Research (STEP) project’ (Grant No. 2019QZKK0208) and the National Natural Science
664 Foundation of China (Grants 41922002 and 41988101-03). We thank Yulong Yang for his
665 assistance with instrument set-up and initial running.

666 **Author contributions**

667 **Niranjan Adhikari**: Data curation, Formal analysis, Writing - Original draft preparation.
668 **Jing Gao**: Data curation, Conceptualization, Methodology, Supervision, Writing - Review and
669 Editing, Funding acquisition. **Aibin Zhao**: measuring assistance, Writing – Editing. **Tianli Xu**,
670 **Manli Chen**, and **Xiaowei Niu**: measuring assistance. **Tandong Yao**: Supervision, Funding
671 acquisition.

672

673

674

675

676 **5 References**

- 677 Acharya, S., Yang, X., Yao, T., Shrestha, D.: Stable isotopes of precipitation in Nepal Himalaya
678 highlight the topographic influence on moisture transport, *Quat. Int.*, 565, 22–30,
679 <https://doi.org/10.1016/j.quaint.2020.09.052>, 2020.
- 680 Adhikari, N., Gao, J., Yao, T., Yang, Y., Dai, D.: The main controls of the precipitation stable
681 isotopes at Kathmandu, Nepal, *Tellus, Ser. B Chem. Phys. Meteorol.*, 72, 1–17.
682 <https://doi.org/10.1080/16000889.2020.1721967>, 2020
- 683 Bohlinger, P., Sorteberg, A., Sodemann, H.: Synoptic conditions and moisture sources actuating
684 extreme precipitation in Nepal, *J. Geophys. Res. Atmos.*, 122, 12–653,
685 <https://doi.org/10.1002/2017JD027543>, 2017.
- 686 Boschi, R., Lucarini, V.: Water pathways for the Hindu-Kush-Himalaya and an analysis of three
687 flood events, *Atmosphere*, 10, 489, <https://doi.org/10.3390/atmos10090489>, 2019.
- 688 Brand, W.A., Geilmann, H., Crosson, E.R., Rella, C.W.: Cavity ring-down spectroscopy versus
689 high-temperature conversion isotope ratio mass spectrometry; a case study on delta (2) H
690 and delta (18) O of pure water samples and alcohol/water mixtures, *Rapid Commun. mass*
691 *Spectrom*, RCM 23, 1879–1884, <https://doi.org/10.1002/rcm.4083>, 2009.
- 692 Breitenbach, S.F.M., Adkins, J.F., Meyer, H., Marwan, N., Kumar, K.K., Haug, G.H.: Strong
693 influence of water vapor source dynamics on stable isotopes in precipitation observed in
694 Southern Meghalaya, NE India, *Earth Planet. Sci. Lett.*, 292, 212–220,
695 <https://doi.org/10.1016/j.epsl.2010.01.038>, 2010.
- 696 Cai, Z., Tian, L.: Atmospheric controls on seasonal and interannual variations in the

697 precipitation isotope in the East Asian Monsoon region, *J. Clim.*, 29, 1339–1352.
698 <https://doi.org/10.1175/JCLI-D-15-0363.1>, 2016.

699 Cai, Z., Tian, L., Bowen, G.J.: Spatial-seasonal patterns reveal large-scale atmospheric controls
700 on Asian Monsoon precipitation water isotope ratios, *Earth Planet. Sci. Lett.*, 503, 158–169.
701 <https://doi.org/10.1016/j.epsl.2018.09.028>, 2018.

702 Chakraborty, S., Sinha, N., Chattopadhyay, R., Sengupta, S., Mohan, P.M., Datye, A.:
703 Atmospheric controls on the precipitation isotopes over the Andaman Islands, Bay of
704 Bengal, *Sci. Rep.*, 6, 1–11, <https://doi.org/10.1038/srep19555>, 2016.

705 Chan, K.T.F., Chan, J.C.L., Zhang, K., Wu, Y.: Uncertainties in tropical cyclone landfall decay,
706 *npj Clim. Atmos. Sci.*, 5, 93, <https://doi.org/10.1038/s41612-022-00320-z>, 2022.

707 Chen, F., Huang, C., Lao, Q., Zhang, S., Chen, C., Zhou, X., Lu, X., Zhu, Q.: Typhoon Control
708 of Precipitation Dual Isotopes in Southern China and Its Palaeoenvironmental Implications,
709 *J. Geophys. Res. Atmos.*, 126, 1–15, <https://doi.org/10.1029/2020JD034336>, 2021.

710 Chhetri, T.B., Yao, T., Yu, W., Ding, L., Joswiak, D., Tian, L., Devkota, L.P., Qu, D.: Stable
711 isotopic compositions of precipitation events from Kathmandu, southern slope of the
712 Himalayas, *Chinese Sci. Bull.*, 59, 4838–4846, <https://doi.org/10.1007/s11434-014-0547-4>,
713 2014.

714 Conroy, J.L., Noone, D., Cobb, K.M., Moerman, J.W., Konecky, B.L.: Paired stable
715 isotopologues in precipitation and vapor: A case study of the amount effect within western
716 tropical Pacific storms, *J. Geophys. Res. Atmos.*, 121, 3290–3303,
717 <https://doi.org/10.1002/2015JD023844>, 2016.

718 Dansgaard, W.: Stable isotopes in precipitation, *Tellus* 16, 436–468,
719 <https://doi.org/10.3402/tellusa.v16i4.8993>, 1964

720 Delattre, H., Vallet-Coulomb, C., Sonzogni, C.: Deuterium excess in the atmospheric water
721 vapour of a Mediterranean coastal wetland: Regional vs. local signatures, *Atmos. Chem.*
722 *Phys.*, 15, 10167–10181, <https://doi.org/10.5194/acp-15-10167-2015>, 2015

723 Draxler, R.R., Hess, G.D.: Description of the HYSPLIT4 modeling system, 1997.

724 Fudeyasu, H., Ichiyanagi, K., Sugimoto, A., Yoshimura, K., Ueta, A., Yamanaka, M.D., Ozawa,
725 K.: Isotope ratios of precipitation and water vapor observed in Typhoon Shanshan, *J.*
726 *Geophys. Res. Atmos.*, <https://doi.org/10.1029/2007JD009313>, 113, 2008.

727 Galewsky, J., Samuels-Crow, K.: Summertime moisture transport to the southern South
728 American Altiplano: Constraints from in situ measurements of water vapor isotopic
729 composition, *J. Clim.*, 28, 2635–2649, <https://doi.org/10.1175/JCLI-D-14-00511.1>, 2015.

730 Galewsky, J., Steen-larsen, H.C., Field, R.D., Risi, W.C., Schneider, M.: Stable isotopes in
731 atmospheric water vapor and application to the hydrologic cycle., *Rev. Geophys.*
732 submitted, 1–169, <https://doi.org/10.1002/2015RG000512>, 2016.

733 Gaona, M.F.R., Villarini, G., Zhang, W., Vecchi, G.A.: The added value of IMERG in
734 characterizing rainfall in tropical cyclones, *Atmos. Res.*,
735 [doi:10.1016/j.atmosres.2018.03.008](https://doi.org/10.1016/j.atmosres.2018.03.008), 209, 95–102, 2018.

736 Gedzelman, S., Lawrence, J., Gamache, J., Black, M., Hindman, E., Black, R., Dunion, J.,
737 Willoughby, H., Zhang, X.: Probing hurricanes with stable isotopes of rain and water vapor,
738 *Mon. Weather Rev.*, [https://doi.org/10.1175/1520-0493\(2003\)131<1112:phwsio>2.0.co;2](https://doi.org/10.1175/1520-0493(2003)131<1112:phwsio>2.0.co;2),

739 131, 1112–1127, 2003.

740 Han, X., Lang, Y., Wang, T., Liu, C.Q., Li, F., Wang, F., Guo, Q., Li, S., Liu, M., Wang, Y., Xu,
741 A.: Temporal and spatial variations in stable isotopic compositions of precipitation during
742 the typhoon Lekima (2019), China. *Sci. Total Environ.*, 762,
743 <https://doi.org/10.1016/j.scitotenv.2020.143143>, 2021

744 Hassenruck-Gudipati, H.J., Andermann, C., Dee, S., Brunello, C.F., Baidya, K.P., Sachse, D.,
745 Meyer, H., Hovius, N.: Moisture Sources and Pathways Determine Stable Isotope Signature
746 of Himalayan Waters in Nepal, *AGU Adv.*, 4, 1–19, <https://doi.org/10.1029/2022av000735>,
747 2023.

748 He, S., Richards, K.: Stable isotopes in monsoon precipitation and water vapour in Nagqu, Tibet,
749 and their implications for monsoon moisture, *J. Hydrol.*, 540, 615–622,
750 <https://doi.org/10.1016/j.jhydrol.2016.06.046>, 2016.

751 Hersbach, H., Bell, B., Berrisford, P., Hirahara, S., Horányi, A., Muñoz-Sabater, J., Nicolas, J.,
752 Peubey, C., Radu, R., Schepers, D.: The ERA5 global reanalysis, *Q. J. R. Meteorol. Soc.*
753 146, 1999–2049, <https://doi.org/10.1002/qj.3803>, 2020

754 Hoffmann, G., Cuntz, M., Jouzel, J., Werner, M.: A systematic comparison between the
755 IAEA/GNIP isotope network and the ECHAM 4 atmospheric general circulation model,
756 *Isot. Water Cycle Past, Present Futur. a Dev. Sci.*, 303–320, 2005.

757 Huffman, G.J., Bolvin, D., Braithwaite, D., Hsu, K., Joyce, R., Kidd, C., Nelkin, E.J.,
758 Sorooshian, S., Tan, J., Xie, P.: Algorithm Theoretical Basis Document (ATBD) of
759 Integrated Multi-satellite Retrievals for GPM (IMERG), version 4.6. Nasa 29, 2017.

760 Hussain, S., Xianfang, S., Hussain, I., Jianrong, L., Dong Mei, H., Li Hu, Y., Huang, W.:
761 Controlling Factors of the Stable Isotope Composition in the Precipitation of Islamabad,
762 Pakistan, *Adv. Meteorol.*, 2015, 1-11, <https://doi.org/10.1155/2015/817513>, 2015.

763 Jackisch, D., Yeo, B.X., Switzer, A.D., He, S., Cantarero, D.L.M., Siringan, F.P., Goodkin, N.F.:
764 Precipitation stable isotopic signatures of tropical cyclones in Metropolitan Manila,
765 Philippines, show significant negative isotopic excursions, *Nat. Hazards Earth Syst. Sci.*,
766 22, 213–226, <https://doi.org/10.5194/nhess-22-213-2022>, 2022.

767 Joseph, S., Freeland, H.J.: Salinity variability in the Arabian Sea, *Geophys. Res. Lett.*, 32,
768 <https://doi.org/10.1029/2005GL022972>, 2005.

769 Kendall, C., Caldwell, E.A.: Fundamentals of Isotope Geochemistry, *Isot. Tracers Catchment*
770 *Hydrol.*, 51–86, <https://doi.org/10.1016/B978-0-444-81546-0.50009-4>, 1998.

771 Kleist, D.T., Parrish, D.F., Derber, J.C., Treadon, R., Wu, W.-S., Lord, S.: Introduction of the
772 GSI into the NCEP global data assimilation system, *Weather Forecast.*, 24, 1691–1705,
773 <https://doi.org/10.1175/2009waf2222201.1>, 2009.

774 Knapp, K.R., Kruk, M.C., Levinson, D.H., Diamond, H.J., Neumann, C.J.: The international best
775 track archive for climate stewardship (IBTrACS) unifying tropical cyclone data, *Bull. Am.*
776 *Meteorol. Soc.*, 91, 363–376, <https://doi.org/10.1175/2009bams2755.1>, 2010.

777 Krishnamurthy, V., Shukla, J.: Intraseasonal and seasonally persisting patterns of Indian
778 monsoon rainfall, *J. Clim.*, 20, 3–20, <https://doi.org/10.1175/jcli3981.1>, 2007.

779 Kurita, N.: Water isotopic variability in response to mesoscale convective system over the
780 tropical ocean, *J. Geophys. Res. Atmos.*, 118, 10,376-10,390,

781 <https://doi.org/10.1002/jgrd.50754>, 2013.

782 Kurita, N., Noone, D., Risi, C., Schmidt, G.A., Yamada, H., Yoneyama, K.: Intraseasonal
783 isotopic variation associated with the Madden-Julian Oscillation, *J. Geophys. Res. Atmos.*,
784 116, 1–20, <https://doi.org/10.1029/2010JD015209>, 2011.

785 Lawrence, J.R., Gedzelman, S.D., Dexheimer, D., Cho, H.K., Carrie, G.D., Gasparini, R.,
786 Anderson, C.R., Bowman, K.P., Biggerstaff, M.I.: Stable isotopic composition of water
787 vapor in the tropics, *J. Geophys. Res. Atmos.*, 109 (D6),
788 <https://doi.org/10.1029/2003jd004046>, 2004.

789 Lawrence, J.R., Gedzelman, S.D., Gamache, J., Black, M.: Stable isotope ratios: hurricane
790 Olivia, *J. Atmos. Chem.*, 41, 67–82, 2002.

791 Lawrence, J.R., Gedzelman, S.D., Zhang, X., Arnold, R.: Stable isotope ratios of rain and vapor
792 in 1995 hurricanes, *J. Geophys. Res. Atmos.*, 103, 11381–11400,
793 <https://doi.org/10.1029/97jd03627>, 1998.

794 Lawrence, R.J., Gedzelman, D.S.: Low stable isotope ratios of tropical cyclone rains, *Geophys.*
795 *Res. Lett.*, 23, 527–530, <https://doi.org/10.1029/96gl00425>, 1996.

796 Lekshmy, P.R., Midhun, M., Ramesh, R.: Role of moisture transport from Western Pacific
797 region on water vapor isotopes over the Bay of Bengal, *Atmos. Res.*, 265, 105895,
798 <https://doi.org/10.1016/j.atmosres.2021.105895>, 2022.

799 Lekshmy, P.R., Midhun, M., Ramesh, R.: Spatial variation of amount effect over peninsular
800 India and Sri Lanka: Role of seasonality, *Geophys. Res. Lett.*, 42(13), 5500–5507,
801 <https://doi.org/10.1002/2015GL064517>, 2015.

802 Lekshmy, P.R., Midhun, M., Ramesh, R., Jani, R.A.: ^{18}O depletion in monsoon rain relates to
803 large scale organized convection rather than the amount of rainfall, *Sci. Rep.*, 4, 1–5.
804 <https://doi.org/10.1038/srep05661>, 2014.

805 Li, L., Chakraborty, P.: Slower decay of landfalling hurricanes in a warming world, *Nature* 587,
806 230–234, <https://doi.org/10.1038/s41586-020-2867-7>, 2020.

807 Li, Z., Yu, W., Li, T., Murty, V.S.N., Tangang, F.: Bimodal character of cyclone climatology in
808 the Bay of Bengal modulated by monsoon seasonal cycle, *J. Clim.*, 26 (3), 1033–1046,
809 <https://doi.org/10.1175/jcli-d-11-00627.1>, 2013.

810 Liebmann, B., Smith, C.A.: Description of a complete (interpolated) outgoing longwave
811 radiation dataset, *Bull. Am. Meteorol. Soc.*, 77, 1275–1277, 1996.

812 Liu, Z., Tian, L., Yao, T., Yu, W.: Seasonal deuterium excess in Nagqu precipitation: Influence
813 of moisture transport and recycling in the middle of Tibetan Plateau, *Environ. Geol.*, 55,
814 1501–1506, <https://doi.org/10.1007/s00254-007-1100-4>, 2008.

815 Midhun, M., Lekshmy, P.R., Ramesh, R.: Hydrogen and oxygen isotopic compositions of water
816 vapor over the Bay of Bengal during monsoon, *Geophys. Res. Lett.*, 40, 6324–6328,
817 <https://doi.org/10.1002/2013GL058181>, 2013.

818 Midhun, M., Pr, L., Ramesh, R., Yoshimura, K., Kk, S.: The effect of monsoon circulation on the
819 stable isotopic composition of rainfall, *J. Geophys. Res. Atmos.*, 123, 5205–5221,
820 <https://doi.org/10.1029/2017JD027427>, 2018.

821 Mohapatra, M., Srivastava, A.K., Balachandran, S., Geetha, B.: Inter-annual variation and trends
822 in Tropical Cyclones and Monsoon Depressions over the North Indian Ocean. Observed

823 Climate Variability and Change over the Indian Region, Springer Geology, 89–106,
824 [https://doi.org/ 10.1007/978-981-10-2531-0_6](https://doi.org/10.1007/978-981-10-2531-0_6), 2016.

825 Munksgaard, N.C., Zwart, C., Kurita, N., Bass, A., Nott, J., Bird, M.I.: Stable isotope anatomy of
826 tropical cyclone Ita, North-Eastern Australia, April 2014, PLoS One 10, 1–15,
827 <https://doi.org/10.1371/journal.pone.0119728>, 2015.

828 Noone, D.: Pairing measurements of the water vapor isotope ratio with humidity to deduce
829 atmospheric moistening and dehydration in the tropical midtroposphere, J. Clim., 25, 4476–
830 4494, <https://doi.org/10.1175/JCLI-D-11-00582.1>, 2012.

831 Pandya, U., Khandelval, S., Sanghvi, H., Joshi, E., Vekaria, G.L., Jaaffrey, S.N.A., Soni, M.:
832 Cyclone ‘TAUKTAE’-Observed through data & satellite images, 2021.

833 Paul, S., Chowdhury, S.: Investigation of the character and impact of tropical cyclone Yaas: a
834 study over coastal districts of West Bengal, India, Saf. Extrem. Environ., 3, 219–235,
835 <https://doi.org/10.1007/s42797-021-00044-y>, 2021.

836 Payne, V.H., Noone, D., Dudhia, A., Piccolo, C., Grainger, R.G.: Global satellite measurements
837 of HDO and implications for understanding the transport of water vapour into the
838 stratosphere, Q. J. R. Meteorol. Soc., 133, 1459–1471, <https://doi.org/10.1002/qj>, 2007.

839 Pfahl, S., Sodemann, H.: What controls deuterium excess in global precipitation? Clim. Past, 10,
840 771–781, <https://doi.org/10.5194/cp-10-771-2014>, 2014..

841 Rahul, P., Ghosh, P., Bhattacharya, S.K., Yoshimura, K.: Controlling factors of rainwater and
842 water vapor isotopes at Bangalore, India: Constraints from observations in 2013 Indian
843 monsoon, J. Geophys. Res., 121, 13,936–13,952, <https://doi.org/10.1002/2016JD025352>,

844 2016.

845 Rajeev, A., Mishra, V.: Observational evidence of increasing compound tropical cyclone-moist
846 heat extremes in India, *Earth's Futur.*, 10, e2022EF002992,
847 <https://doi.org/10.1029/2022ef002992>, 2022.

848 Risi, C., Bony, S., Vimeux, F.: Influence of convective processes on the isotopic composition
849 ($\delta^{18}\text{O}$ and δD) of precipitation and water vapor in the tropics: 2. Physical interpretation of
850 the amount effect, *J. Geophys. Res. Atmos.*, 113, 1–12,
851 <https://doi.org/10.1029/2008JD009943>, 2008.

852 Sánchez-Murillo, R., Durán-Quesada, A.M., Esquivel-Hernández, G., Rojas-Cantillano, D.,
853 Birkel, C., Welsh, K., Sánchez-Llull, M., Alonso-Hernández, C.M., Tetzlaff, D., Soulsby,
854 C., Boll, J., Kurita, N., Cobb, K.M.: Deciphering key processes controlling rainfall isotopic
855 variability during extreme tropical cyclones, *Nat. Commun.*, 10, 1–10,
856 <https://doi.org/10.1038/s41467-019-12062-3>, 2019.

857 Saranya, P., Krishan, G., Rao, M.S., Kumar, S., Kumar, B.: Controls on water vapor isotopes
858 over Roorkee, India: Impact of convective activities and depression systems, *J. Hydrol.*,
859 557, 679–687, <https://doi.org/10.1016/j.jhydrol.2017.12.061>, 2017.

860 Singh, A., Jani, R.A., Ramesh, R.: Spatiotemporal variations of the $\delta^{18}\text{O}$ –salinity relation in the
861 northern Indian Ocean, *Deep Sea Res., Part I* 57 (11), 1422–1431,
862 <https://doi.org/10.1016/j.dsr.2010.08.002>, 2010.

863 Steen-Larsen, H.C., Sveinbjörnsdóttir, A.E., Peters, A.J., Masson-Delmotte, V., Guishard, M.P.,
864 Hsiao, G., Jouzel, J., Noone, D., Warren, J.K., White, J.W.C.: Climatic controls on water

865 vapor deuterium excess in the marine boundary layer of the North Atlantic based on 500
866 days of in situ, continuous measurements, *Atmos. Chem. Phys.*, 14, 7741–7756,
867 <https://doi.org/10.5194/acp-14-7741-2014>, 2014.

868 Sun, C., Tian, L., Shanahan, T.M., Partin, J.W., Gao, Y., Piatrunia, N., Banner, J.: Isotopic
869 variability in tropical cyclone precipitation is controlled by Rayleigh distillation and cloud
870 microphysics, *Commun. Earth Environ.*, 3, <https://doi.org/10.1038/s43247-022-00381-1>,
871 2022.

872 Tian, L., Masson-Delmotte, V., Stievenard, M., Yao, T., Jouzel, J.: Tibetan Plateau summer
873 monsoon northward extent revealed by measurements of water stable isotopes, *J. Geophys.*
874 *Res.*, 106, 28081–28088, <https://doi.org/10.1029/2001JD900186>, 2001.

875 Tian, L., Yu, W., Schuster, P.F., Wen, R., Cai, Z., Wang, D., Shao, L., Cui, J., Guo, X.: Control
876 of seasonal water vapor isotope variations at Lhasa, southern Tibetan Plateau, *J. Hydrol.*,
877 580, 124237, <https://doi.org/10.1016/j.jhydrol.2019.124237>, 2020.

878 Tian, L., Yao, T., Numaguti, A., Sun, W.: Stable isotope variations in monsoon precipitation on
879 the Tibetan Plateau, *J. Meteorol. Soc. Japan.*, 79, 959–966,
880 <https://doi.org/10.2151/jmsj.79.959>, 2001.

881 Uemura, R., Matsui, Y., Yoshimura, K., Motoyama, H., Yoshida, N.: Evidence of deuterium
882 excess in water vapor as an indicator of ocean surface conditions, *J. Geophys. Res. Atmos.*,
883 113, <https://doi.org/10.1029/2008jd010209>, 2008.

884 Verma, K., Gupta, A., 2021. *Cyclone Tauktae: Cyclones, Their Impacts and Disasters Risk*
885 *Management*.

886 Villarini, G., Smith, J.A., Baeck, M.L., Marchok, T., Vecchi, G.A.: Characterization of rainfall
887 distribution and flooding associated with US landfalling tropical cyclones: Analyses of
888 Hurricanes Frances, Ivan, and Jeanne (2004), *J. Geophys. Res. Atmos.*, 116, <https://doi.org/10.1029/2011jd016175>, 2011.

890 Wei, Z., Yoshimura, K., Okazaki, A., Ono, K., Kim, W., Yokoi, M., Lai, C.T.: Understanding
891 the variability of water isotopologues in near-surface atmospheric moisture over a humid
892 subtropical rice paddy in Tsukuba, Japan, *J. Hydrol.*, 533, 91–102,
893 <https://doi.org/10.1016/j.jhydrol.2015.11.044>, 2016.

894 Worden, J., Noone, D., Bowman, K.: Importance of rain evaporation and continental convection
895 in the tropical water cycle, *Nature*, 445, 528–532, <https://doi.org/10.1038/nature05508>,
896 2007.

897 Xu, T., Sun, X., Hong, H., Wang, X., Cui, M., Lei, G., Gao, L., Liu, J., Lone, M.A., Jiang, X.:
898 Stable isotope ratios of typhoon rains in Fuzhou, Southeast China, during 2013–2017, *J.*
899 *Hydrol.*, 570, 445–453, <https://doi.org/10.1016/j.jhydrol.2019.01.017>, 2019.

900 Yoshimura, K.: Stable Water Isotopes in Climatology, Meteorology, and Hydrology: A Review,
901 *J. Meteorol. Soc. Japan*, 93, 513–533, <https://doi.org/10.2151/jmsj.2015-036>, 2015.

902 Yu, W., Yao, T., Tian, L., Ma, Y., Ichiyanagi, K., Wang, Y., Sun, W.: Relationships
903 between $\delta^{18}\text{O}$ in precipitation and air temperature and moisture origin on a south-north
904 transect of the Tibetan Plateau, *Atmos. Res.*, 87, 158–169,
905 <https://doi.org/10.1016/j.atmosres.2007.08.004>, 2008.

906 Yu W, Yao T, Tian L, Ma Y, Wen R, Devkota LP, Wang W, Qu D, Chhetri TB.: Short-term
907 variability in the dates of the Indian monsoon onset and retreat on the southern and northern
908 slopes of the central Himalayas as determined by precipitation stable isotopes, *Clim. Dyn.*,
909 47, 159-72, <https://doi:10.1007/s00382-015-2829-1>, 2016.

910

911

912